Nano Energy 147 (2026) 111597

Contents lists available at ScienceDirect

Nano Energy

journal homepage: www.elsevier.com/locate/nanoen

Full paper

Multi-phase characterization of pitch-carbon coated nano-silicon anodes for lithium-ion batteries

Kae E. Fink, Peter J. Weddle, Jack R. Palmer[1], Christof Zweifel[2], Glenn Teeter, Ankit Verma, Shane Frisco[3], Sang-Don Han[4], Maxwell C. Schulze, G. Michael Carroll, Andrew M. Colclasure, Nathan R. Neale, Bertrand J. Tremolet de Villers *

National Renewable Energy Laboratory, Golden, CO 80401, USA

ARTICLE INFO

Keywords:
Lithium-ion battery
Silicon anode
Pitch carbon coating
Solid-electrolyte interphase (SEI) reactivity
Multi-phase characterization

ABSTRACT

Silicon (Si) is a leading next-generation Li-ion battery anode candidate that meets rigorous performance demands for portable power including enhanced power and energy density with robust cycling performance. However, a series of complex and interrelated reactions lead to reduced calendar life in Si-containing systems and therefore challenge practical adoption. In the present work, we probe the mechanisms underlying observed performance improvements by adding a pitch-carbon coating onto nano-Si material. We pair solid-phase (X-ray photoemission spectroscopy, Fourier-transform infrared), semi-volatile phase (solid-phase microextraction–gas chromatography-mass spectrometry), and gas-phase (gas chromatography-flame-ionization detector) characterization signals to comprehensively evaluate the impact of pitch-carbon coating on the evolution of the Si solid-electrolyte interphase (SEI) and the associated impacts on electrode/electrolyte reactivity. The pitch-carbon is found to serve as a physicochemical barrier, reducing the electro-active surface area for Si/electrolyte reactivity and preventing Si oxidation. Further, the pitch-carbon coating promotes the evolution of a more-favorable SEI by subsuming substantial functionality typically associated with the fluoroethylene carbonate (FEC) electrolyte additive – such as alkoxide scavenging and suppression of transesterification pathways – and by shifting the competitive electrolyte degradation pathways' favorability. The multi-phase characterization approach enables holistic end-products evaluation from complex (electro)chemical interfacial reactions, which informs a robust interpretation of the carbon coating's role in electrochemical performance improvements. The present mechanistic evaluation aids the rational design for improved nano-Si materials.

1. Introduction

Over the past several years, demand has surged for next-generation battery materials that provide high power and increased energy density with superior cycling and calendar life capabilities. Silicon (Si) is a promising Li-ion anode material candidate that meets these rigorous performance demands, given its high theoretical capacity of 3579 mAh g^{-1} (nearly 10x that of graphite, for $Li_{15}Si_4$), a relatively low lithiation potential window of ≈0.1–0.01 V vs. Li^+/Li [1], and high earth abundance, which offers enhanced supply chain security relative to battery-grade graphite. While leading Si anode battery chemistries demonstrate promising cycle life [2], a series of complex and interrelated side reactions lead to reduced calendar life [3], impeding practical material adoption.

During cycling, Si undergoes volume changes of ≈280-300% [1,4], which induces high mechanical stresses in Si particles and leads to particle fracture [1,5]. Nanostructuring Si can mitigate the mechanical failure modes observed during electrochemical cycling [1], and particle fracture can be mostly avoided below a critical size threshold of ≈150 nm. [6,7].

However, in the nanosized regime where mechanical failure modes are largely suppressed, Si is plagued by complex interfacial surface reactivity, which is exacerbated by the high surface area. Unprotected

* Corresponding author.
E-mail address: Bertrand.Tremolet@nrel.gov (B.J. Tremolet de Villers).
[1] Present address: Materials Science and Engineering Program, University of California, San Diego, 9500 Gilman Drive, La Jolla, CA 92093, USA.
[2] Present address: School of Earth & Environmental Sciences, University of Minnesota, Suite 150, 116 Church St SE, Minneapolis, MN 55455, USA.
[3] Present address: Forge Nano, 12300 Grant St #110, Thornton, CO 80241, USA.
[4] Present address: Department of Chemistry, Sejong University, Seoul 05006, Republic of Korea.

https://doi.org/10.1016/j.nanoen.2025.111597
Received 3 July 2025; Received in revised form 13 November 2025; Accepted 15 November 2025
Available online 19 November 2025

("bare") Si demonstrates adverse reactivity – both chemical and electrochemical – when exposed to carbonate solvents. Bare Si has been shown to spontaneously react with standard battery electrolytes containing $LiPF_6$ and carbonate solvents, forming an interfacial layer rich in Si–O–F and C–O–H–F type species even in the absence of an applied potential [8]. Lithiated Si shows even greater chemical reactivity. For example, nuclear magnetic resonance (NMR) studies suggest that $Si^{2-/4-}$ anions in the Li-Si Zintl phase can serve as pseudo-nucleophiles, driving reductive decomposition of carbonates at electrophilic sites and can concurrently form dimers or clusters of Si [9].

Electrochemical (i.e., potential-driven) Si reactivity with carbonate solvents to form the electronically insulating/ionically conductive solid-electrolyte interphase (SEI) has also been extensively reported [8,10–14]. The precise composition, structure, morphology, and arrangement of SEI species is functionally dependent on electrode chemistry, electrolyte composition, counter-electrode identity, applied potential, temperature, etc. [15]. Notably, the same standard electrolyte (e.g., carbonate solvents with $LiPF_6$ salt) that produces an effectively passivating SEI on graphite does not act analogously with Si. Instead, these standard electrolytes undergo continuous adverse reactions to form a poorly passivating SEI [16,17], the growth of which is exacerbated by repeated expansion/contraction during cycling that exposes fresh lithium silicide surfaces [18].

Electrolyte additives that improve Si anode performance have been well-documented [19], with fluoroethylene carbonate (FEC) being perhaps the most commonly reported [17,18,20–22]. The nominal reduction potential of FEC is ≈0.3 V more positive than that of ethylene carbonate and preferential reduction of FEC in Si systems forms a reportedly "better" SEI [17]. Performance improvements in FEC-containing electrolytes have, in part, been attributed to the formation of a heterogeneous, cross-linked polymeric SEI that offers enhanced flexibility, which is particularly beneficial for high-volume-expansion Si materials [17,18,20]. FEC also contributes to the evolution of a thinner–yet more effectively passivating–SEI [17].

Further, SEI-forming reactions at the Si surface depend on the termination chemistry [13]. Several methods, including pyrolytic carbon and pitch-carbon carbon coating, have been demonstrated to improve the electrochemical performance of silicon anodes [23,24]. For nanosized Si, tuning the Si surface chemistry with molecular coatings has been shown to drastically influence surface stability and associated electrochemical cycling performance [25]. Without such surface coatings, hydride-terminated nano-Si (i.e., SiH_x, where $x = 1, 2, 3$) is practically unviable due to the highly reactive hydride moiety and large total surface area. Modifying SiH_x with a variety of covalently attached surface coatings is a proven strategy to minimize adverse chemical reactivity and mimic beneficial properties of the SEI. Several distinct classes of interfacial coatings have been explored [2,25,26], including physical mixtures of nanosized Si and an sp^2-carbon-rich polycyclic aromatic hydrocarbon matrix derived from petroleum pitch [27]. In this promising **Si-Pitch** system (investigated further in the present study), capacity retention and coulombic efficiency improvements are in large part attributed to suppressed parasitic reactions at the electrode/electrolyte interface as compared to an "uncoated" **Si-NMP** analog (also investigated further in the present study), where N-methyl-2-pyrrolidone (NMP) is the processing solvent for the uncoated Si particles that spontaneously reacts with the hydride-terminated nano-Si surface to form a covalently bound NMP-derived molecular coating. However, a robust (electro)chemically informed rationale for this observed performance improvement has yet to be reported.

Developing a holistic understanding of SEI evolution – for any electrode material – is complicated by the inherently three-phase nature and potential dependence of reactions driving SEI growth. The vast majority of SEI studies conducted to date on Si materials have relied predominantly on characterization conducted in the solid phase [8,13,14,17,18,20,26,28–35]. Since the SEI evolves primarily from electrolyte reduction species, evaluating the liquid phase also yields valuable insights into the SEI evolution processes. While liquid-phase analysis is typically conducted post-mortem [36] or by soaking recovered cell components [37]), volatile-phase preconcentration methods such as solid-phase microextraction (SPME) have also been employed to evaluate electrolyte compositional changes in situ [38]. Finally, methods using gas-phase signals to probe SEI evolution are a critical, though still relatively under-studied, complement to more common solid- and liquid-phase approaches. The predominantly oxide and hydrocarbon gases evolved during electrolyte reduction can offer both qualitative and quantitative insights into mechanistic pathways of reactivity [13,16,39–41].

Even for a single material under a single set of operating conditions, dozens of competing reactive pathways govern electrolyte degradation and SEI growth [42], many producing comparable products. Due to the immense and convoluted complexity of this challenge, workflows to analyze SEI evolution typically aim to elucidate one particular pathway, and/or emphasize characterization in predominantly one phase. In this way, individual input signals can be combined and extrapolated to build plausible complete mechanisms of reactivity. However, using coupled characterization methods across all three phases, as in the present work, provides a more complete picture of reactivity that is unachievable by evaluating each phase in isolation.

We herein take a holistic, multi-phase approach to analyzing the electrochemical degradation processes that impact Si calendar life in a promising nano-Si composite material. We focus our study on a recently reported novel Si-Pitch composite material, whereby nanosized Si ($d = 5.9$ nm) particles are coated with carbon extracted from petroleum pitch. This Si-Pitch material has drastically improved cycling performance as compared to unprotected nano-Si and is a promising candidate to achieve improved Si calendar life [27]. We have previously demonstrated that powders of each material produce substantially distinct gas speciation when soaked in electrolyte [27]. In the present work, we expand our analysis and utilize coupled in situ and ex situ methods to probe changes to solid-surface, volatile headspace, and gas-phase chemistry occurring during initial cell cycling. Complementary measurements are taken at targeted cell potentials associated with specific electrolyte species reduction, decoupling the reaction pathways tied to interfacial stability.

Our coupled characterization approach suggests that pitch serves two dominant purposes, as shown schematically in Fig. 1: (1) Pitch serves as a physicochemical barrier to reduce active Si area exposed the electrolyte, and thereby lessens Si oxidation; (2) The conjugated carbon network in pitch favors the evolution of a more favorable SEI by (i) subsuming the role and functionality of the electrolyte additive FEC and (ii) altering the balance of competitive electrolyte reduction pathways. Each of these functionalities are expected to contribute to the observed performance improvement, and each will be presented and discussed in detail. The design principles revealed in this work – i.e., how pitch facilitates a "better" SEI – are critical to informing the rational and accelerated design of improved nano-Si materials and surface coatings.

2. Materials and methods

2.1. Electrode and cell preparation

Silicon nanoparticles were synthesized by plasma enhanced chemical vapor deposition according to our previously described methods [26,27,43]. Si nanoparticles (D50 = 5.9 nm) recovered from the plasma reactor were functionalized with N-methyl-2-pyrrolidone (NMP) using previously reported methods [26]. A portion of the resulting material was retained for processing into Si-NMP electrodes.

Si-Pitch material was also prepared using previously reported methods [27]. Briefly, Si-Pitch slurries were prepared under an inert argon atmosphere by ball-milling 8 mass equivalents of Si-Pitch powder with 1 mass equivalent of Timcal C65 conductive carbon. A 10 wt% solution

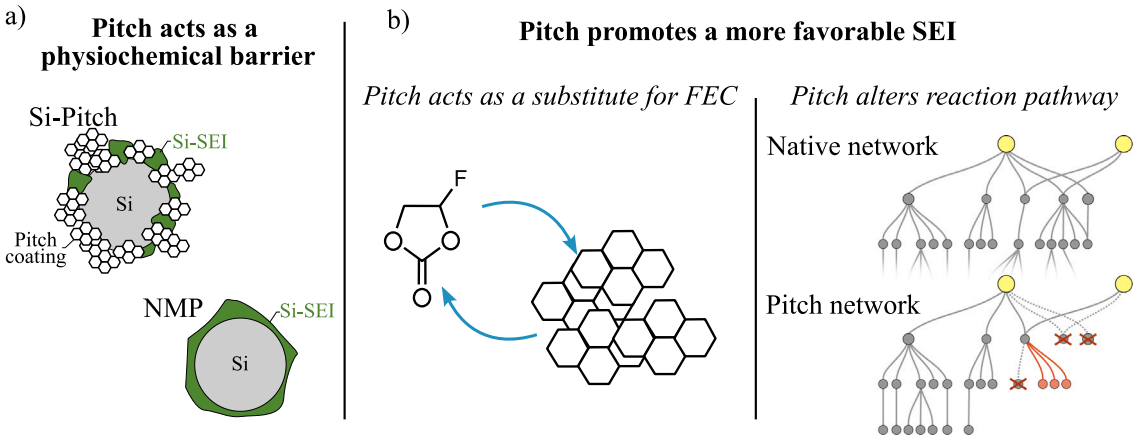

Fig. 1. Schematic representation of proposed mechanisms by which pitch-carbon coating enhances the electrochemical performance of nano-Si. These mechanisms are taken up in detail in Section 3.

of P84 polyimide (Tecapowder PI, Ensinger Sintimid GmbH) in NMP was then added to each mixture in a screwcap scintillation vial such that the final slurry of Si-Pitch contained the following ratio: Si-Pitch–80:10:10 by mass of Si-Pitch powder, Timcal C45, and P84 polyimide, respectively.

Si-NMP slurries were similarly prepared in an Ar-filled glovebox. Si-NMP particles were dispersed in NMP; the mixture was sonicated for 10 min in a bath sonicator and was subsequently stirred for four hours at 100 °C. After the initial dispersion was formed, Timcal C65 was added to the mixture and was then stirred overnight at 100 °C. Finally, a 10 wt% solution of P84 polyimide in NMP was added to the mixture and the suspension was then stirred at 50 °C for an hour. The final slurry of Si-NMP contained 60:20:20 by mass of Si-NMP nanoparticles:Timcal C45:P84 polyimide. Each slurry was mixed with a Mazerustar KK-250S planetary mixer using 3 mm glass bead mixing media and was subsequently cast onto the rough side of 25 μm Cu foil current collector using a doctor blade (wet gap of 100 μm for Si-NMP electrodes and 70 μm for Si-Pitch electrodes to achieve an approximate loading of ≈1.1 mg cm^{-2} for Si-NMP electrodes and ≈1.8 mg cm^{-2} for Si-Pitch electrodes). The Si-NMP electrode was dried at 420 °C for 4 h under 0.5 L min^{-1} of flowing nitrogen gas. The Si-Pitch electrode was dried under vacuum at 150 °C for 4 h.

Half-cells were prepared in standard CR2032 format for current decay measurements and solid-phase surface analysis. Each half cell contained a 14 mm diameter punch of Si anode (Si-NMP or Si-Pitch cast onto Cu foil) with a 15 mm diameter Li foil reference and a 19 mm diameter Celgard 2325 separator. A total of 40 μL GenF-10 electrolyte (1.2 M $LiPF_6$ in 3:7 ethylene carbonate:ethylmethyl carbonate (EC:EMC) by weight, with a total of 10 wt% FEC additive) was added to each cell.

All reported gas analysis tests were conducted in half-cell format using a PAT Gas Cell (El-Cell GmbH) assembled in an Ar gas glovebox. Figure S1a depicts the gas-cell component configuration. In each cell, a 14 mm anode (Si-NMP or Si-Pitch cast onto Cu foil) was placed directly onto the lower plunger (flow field) of the gas cell. 100 μL of freshly prepared GenF-10 electrolyte was added dropwise onto the active surface of the anode. The cell separator (Celgard 2325; 21 mm) was immobilized in a polypropylene insulation sleeve specifically designed to enable a gas-tight seal within the gas cell. This insulation sleeve contained a 316L stainless steel clamping ring with no reference ring; components were obtained in disassembled form from El-Cell GmbH and then press-fit into place. An additional 10 μL of GenF-10 was added dropwise on top of the separator, followed by a disc of Li foil (15 mm, Sigma-Aldrich) that had been gently surface-cleaned using a clean spatula to remove the native oxide and any surface impurities. Finally, the upper plunger was centered on the stack and the gas cell was sealed to finger-tight pressure prior to removing from the glovebox.

2.2. Electrochemical cycling

To probe electrochemical evolution of gaseous species, a voltage-hold protocol was developed whereby the cell was held at different potentials associated with electrochemical reduction processes previously reported in the literature for GenF-10 electrolyte. It should be noted that, in accordance with a recent report [44], this voltage-hold protocol has not been applied to predict (either qualitatively or quantitatively) the calendar lifetime of the Si material under study. Rather, the voltage-hold technique has been applied at each potential of interest in lieu of a single time-resolved measurement to drive the dominant reactive pathways at each potential, thereby enabling evaluation of voltage-dependent electrochemical reaction. The data reported therefore reflects an individual cell that was held at the given potential. Due to the highly intensive nature of cell fabrication and testing and the standardized cell assembly protocol, tests run in the gas cell comprised of a single sample at each reported potential. Further details on voltage-hold data treatment are discussed in the Supplementary Material.

For both gas-cell and coin-cell tests, the voltage-hold protocol consisted of a 5 hr initial rest at the open circuit voltage, followed by applying a C/10 constant current (current rate determined by the nominal mass loading of each Si electrode, which were individually weighed) and a 180 h constant voltage hold. For Si-Pitch electrodes, the voltage hold was conducted at 1500 mV; 800 mV; 400 mV; or 50 mV during the first lithiation; additional measurements were conducted at open-circuit voltage (OCV) prior to lithiation. Figure S1b illustrates the voltage-hold protocol and highlights all measurement points. For Si-NMP electrodes, a subset of the measurement points were selected during the initial lithiation cycle (1500 mV, 800 mV, and 50 mV). Following the 180 h voltage hold, cells were allowed to relax to their open circuit potential.

2.3. Material characterization-solid phase

Following the voltage-hold protocol described above and in the Supplementary Material, coin cells were disassembled for solid-state surface analysis. Prior to FTIR and XPS analysis, recovered electrode samples were soaked in 1 mL of dimethyl carbonate (DMC) for 1 min. This mild surface rinsing was conducted to remove residual electrolyte, which has previously been found to interfere with surface analysis, while minimizing disruptive alterations to the native SEI.

FTIR spectra were measured using a Bruker Alpha II spectrometer equipped with a germanium attenuated total reflectance (ATR) accessory. The spectrometer was situated inside an argon glovebox with < 0.5 ppm H_2O and < 0.5 ppm O_2. Scans were collected between

4000–600 cm^{-1}. The glovebox atmosphere (Ar gas) was measured as the reference blank prior to sample measurements. Reported spectra reflect an average of 192 acquisitions. Spectra were baseline subtracted using a convex-hull fitting function.

XPS measurements were performed in a Physical Electronics Phi VersaProbe III instrument using Al-ka excitation (hn = 1486.7 eV). High-resolution core-level spectra were collected at a pass energy of 55 eV. Prior to XPS measurements, effects of surface contamination were minimized by handling and transferring samples only under controlled-ambient (Ar) conditions. XPS spectra were curve-fitted using customized procedures in Igor Pro, with appropriate constraints applied to ensure peak-area proportionality and constant binding-energy separations for all elements within a given phase across different core-level spectra.

2.4. Material characterization–semi-volatile and gaseous headspace

Semi-volatile and gaseous headspace products evolved during cycling were analyzed using an Agilent 7890B gas GC paired with an Agilent 5977B mass spectrometer (MS) and an Agilent flame-ionization detector (FID) with methanizer. The GC was outfitted with two parallel stationary columns of proprietary composition optimized for the separation of electrolyte components (Column 1: 30 m × 0.25 mm; Column 2: 60 m × 0.53 mm; Wasson-ECE). During SPME analysis, the sample was only analyzed via Column 1 and the MS detector. During direct gas analysis, sample volume was split between the two columns, such that the first column separated and directed samples through the MS detector, while the second column separated and directed samples through the FID detector. The split ratio between MS and FID columns remained constant throughout sample analysis. Specific preparation and analysis methods for SPME and direct gas measurements are detailed below.

Ex situ analysis of the separator recovered from coin cells was used to evaluate the semi-volatile headspace products evolved at each potential. Immediately after opening the coin cell in an Ar-gas glove box, the wet separator was placed into a 1 mL polypropylene vial, then sealed with a PTFE-lined crimp cap (Agilent). An 85 μm polyacrylate-coated fused silica SPME fiber (24 gauge; Supelco) was inserted into the sample vial headspace for 8 min at room temperature (≈22 °C), during which volatile and semi-volatile species adsorbed onto the fiber. The 8 min headspace dwell time was selected following measurement of a representative sample of GenF-10 electrolyte, whereby linearity of the SPME signal was demonstrated up to a maximum intensity at 8 min of headspace dwell time (Figure S2). The SPME fiber was subsequently desorbed in the GC inlet at 270 °C for 1 min. Helium was used as carrier gas (1.16 mL min^{-1} column flow and 8.85 psi column pressure) and the GC was run in splitless mode according to the following protocol (adapted from [38]): from a starting temperature of 40 °C, the temperature was increased at a rate of 3 °C min^{-1} to 60 °C; then increased at a rate of 30 °C min^{-1} until a final temperature of 260 °C was reached. Chemical species eluting from the column were continuously measured by the MS detector.

For El-Cell samples, the volatile headspace was evaluated in situ at the end of the voltage hold period (≈174 h) via diluted direct gas extraction. A gas-tight syringe filled with 8 mL of Ar gas was used to slowly (≈10 s) introduce the dilution gas volume through the inlet port of the El-Cell; simultaneously, a second syringe connected to the outlet port (initially evacuated) was used to withdraw 8 mL of gas, which contained the cell headspace product gas diluted in the Ar dilution gas. Figure S1a illustrates the schematic setup. A dilutant was required to fill the minimum sample volume loop on the GC and enable simultaneous MS and FID analysis.

Prior to each analysis, a blank sample containing 8 mL of Ar gas from the same source used for sample dilution was analyzed via GC-MS-FID; this blank was used to both verify column purity and as a basis for background-subtraction of peak intensities to account for minor fluctuations in the background Ar signal. Following the blank run, 8 mL of sample gas (El-Cell headspace diluted in Ar) was introduced onto the GC-MS-FID. Helium was used as carrier gas (18.3 psi column pressure) and the GC was run according to a previously established and reported protocol [27]: briefly, a starting temperature of 40 °C was held for 3 min; the temperature was increased at a rate of 18 °C min^{-1} to 200 °C; and the final temperature of 200 °C was held for 5 min. The FID was operated at 200 °C with the methanizer temperature set at 450 °C; H_2 and air flows for the FID were set at 25 and 450 mL min^{-1}, respectively.

The gaseous species herein reported were evaluated primarily through FID. Given that FID does not inherently enable product identification, a series of qualitative identification runs were performed to determine the identity of each detected gaseous product. Specifically, 8 mL of each of a series of high-purity gaseous standards (GASCO, Calgas Direct) was introduced onto the column. The standards were analyzed using the same instrumental method described above, such that the retention time of the standard gas could be matched to observed retention times in the sample chromatogram.

Table 1
Potential-hold voltages selected for this study. Voltages were selected to be slightly below the literature-reported nominal reduction potential of various electrolyte species or relevant reduction events [18,20,22] and also correspond to differential capacity features observed in half-cell cycling of Si-Pitch (Figure S1b).

Potential vs Li^+/Li	Dominate electrochemical reduction event
Open circuit	N/A (pure chemical reactivity)
1.5 V	$LiPF_6$ decomposition*
0.8 V	FEC decomposition
0.4 V	EC decomposition
0.05 V	Si lithiation

*Reported in the presence of trace H_2O [49] or as spontaneous bond breaking [22].

3. Results and discussion

3.1. Reduced electrochemical reactivity of pitch-carbon-coated Si nanoparticles

For novel electro-active materials (including Si composites), the relative magnitude of adverse electrochemical reactivity can be qualitatively identified through a potentiostatic hold, whereby the residual current measured throughout a long (≈180 h) voltage hold is related to side reactions in the cell [44–47]. This approach is discussed in detail in the Supplementary Material. Previously, our team demonstrated reduced parasitic reactivity of Si-Pitch electrodes relative to Si-NMP material at an operationally relevant lithiation potential of 10 mV, as evidenced by lower residual current values in the Si-Pich system [27]. In the present work, the analysis has been expanded to four distinct voltage-hold potentials, which are applied in Si-composite/Li half cells. This approach to evaluating voltage-resolved reactivity has previously been used to evaluate SEI growth and passivation in Si thin-film systems [48]. Voltage-hold potentials were selected just below notable differential capacity features observed during half-cell cycling of the Si-Pitch material (Figure S1b-c). These potentials are listed in Table 1, along with assignments of the predominant redox event predicted to occur at each potential based on previous literature reports [18,20,22].

For both Si-NMP and Si-Pitch cells, model fits according to Eq. S3 show good agreement with experimentally observed capacities during the latter portion of the voltage hold. In Fig. 2, model fits are shown presuming a maximum lithiation onset of 100 h ($t_{rev,max}$ = 100 h; i.e., fitting the last 80 h of capacity data). Varying the maximum lithiation onset time between 80 and 130 h does not substantially improve the quality of fit (Figures S3 and S4).

Fig. 2 shows the normalized currents during the voltage holds for Si-NMP versus Si-Pitch at potentials ranging from 1500 mV to

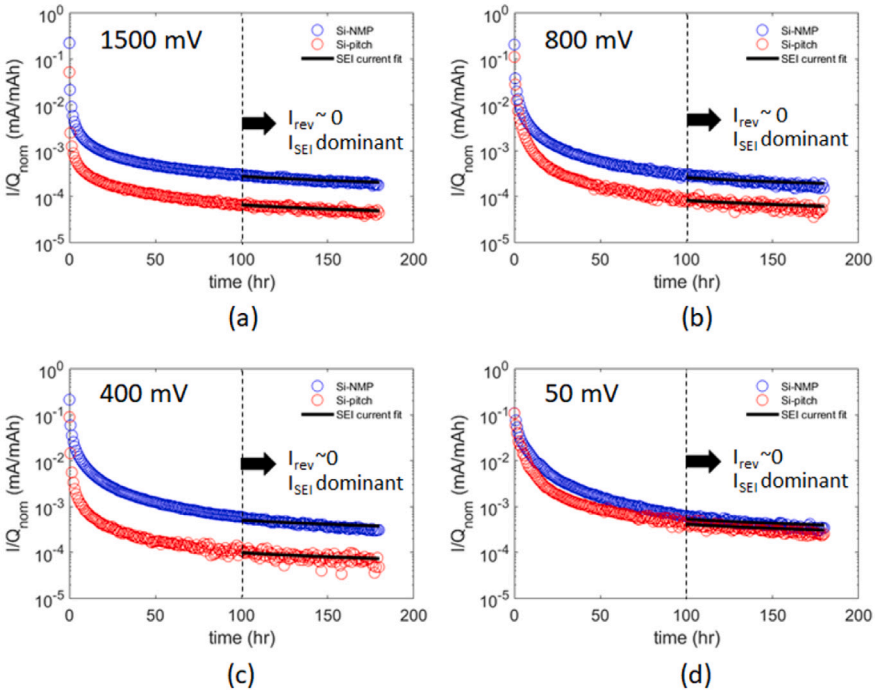

Fig. 2. Normalized current decay profiles of Si-Pitch and Si-NMP coin cells during a 180 hr voltage hold at 4 potentials of interest: (a) 1500 mV, (b) 800 mV, (c) 400 mV and (d) 50 mV. Model fits to capacity according to Eq. S3 are shown for $t_{rev,max}$ = 100 h.

50 mV as well as the associated model fits. For each Si composite material (Si-NMP and Si-Pitch), currents have been normalized to the nominal capacity achieved during lithiation to 50 mV. This ensures appropriate comparison between the relative magnitudes of residual current for the two material types. Voltage-hold data fit statistics are presented in Table S1. Consistent values for the fit parameter reflecting temporal growth of the SEI (see details in the Supplementary Material) are obtained across all fit replicates, with a maximum coefficient of variation of 7.67% and 5% for Si-NMP and Si-Pitch, respectively (Figure S5). The maximum coefficient of variation is observed for the 50 mV hold where highest reversible lithiation occurs.

In all sub-plots of Fig. 2, the normalized total current associated with the Si-Pitch cells lie below that of the Si-NMP cells, suggesting that Si-NMP has higher parasitic currents than Si-Pitch at all voltage-hold potentials. The trend of higher SEI currents at lower hold-potentials is also observed for both samples. This confirms previous reports of improved interfacial passivation induced by the pitch-carbon coating and suggests that the passivation mechanism is at least in part electrochemical, i.e., potential-dependent. However, the voltage-hold method only tracks electrochemical contributions to parasitic reactivity and cannot explicitly probe or quantify chemical reactivity (i.e., reactions occurring in the absence of applied potential). Further, it is challenging to determine from voltage-hold analyses alone whether pitch has a beneficial impact above and beyond that of simply reducing the exposed total surface area of bare Si. A more detailed analysis is needed to explain the role of pitch in facilitating a highly performing and surface-stable nano-Si electrode.

3.2. Pitch acts as a physicochemical barrier

Perhaps the simplest explanation for the beneficial impacts imparted by pitch-carbon coating is that the pitch serves as a physicochemical barrier between the reactive nano-Si and electrolyte. Spontaneous reactions of electrolyte with bare Si have been reported even in the absence of applied potential [8,50]. Such adverse chemical reactivity is exacerbated in lithiated Si systems, where nucleophilic $Si^{2-/4-}$ species drive reductive electrolyte decomposition [9]. Uncoated silicon's potential-dependent reactivity with carbonate solvents has also been extensively reported [8,10–14]. Thus, there is a strong case for the notion that reducing the active Si surface area, such as through pitch-carbon coating, should limit reactivity by minimizing Si/electrolyte interactions.

We have previously demonstrated that pitch-carbon forms a heterogeneous surface coating on nano-Si [27], indicating that the total area of potentially reactive Si is reduced but not fully eliminated for the pitch-coated system (see for example, scanning transmission electron miscroscope-energy dispersive spectroscopy in Figure S4 in [27]). By this "physicochemical barrier" explanation, the pitch carbon would be expected to protect the nano-Si, reducing adverse (electro)chemical electrolyte degradation and simultaneously preserving the Si chemistry and structure. Coupled solid-state analysis using FTIR (Fig. 3 and Figure S6) and XPS (Fig. 4) support these conclusions. Both techniques indicate that the pitch-carbon coating facilitates SEI passivation at higher potentials relative to the baseline NMP coating. FTIR spectra of the Si anodes recovered from half cells after 180 h voltage holds at each of the potentials listed in Table 1 are shown in Fig. 3. The spectrum of a pure P84 binder film is also included for reference (gray trace). The P84 binder has several distinct IR absorption peaks including at 1724, 1512, 1360, 1100, and 720 cm^{-1}. Most of these peaks are still present in the OCV (2230 mV) and 1500 mV samples. However, at 800 mV and below, the P84 peaks are diminished significantly, indicating surface coverage. The observed reduction in P84 signal occurs concurrently with an increase in typical SEI species at 1840–1740 cm^{-1} (oligomeric vinylene or fluoroethylene carbonates), 1660–1620 and 1460 cm^{-1} (lithium alkyl carbonate) [28,32,51], 1590 cm^{-1} (lithium carboxylates, asymmetric) [28], 1490 cm^{-1} and 1440 cm^{-1} (lithium carbonate) [28,32], 1320 cm^{-1} (carboxylate, symmetric), 1070 cm^{-1} (lithium alkoxide) [33,52], and 870–850 cm^{-1} (lithium carbonate). In Fig. 3, it is evident that at all cell potentials higher than 50 mV, the Si-Pitch samples show much less signal overall as compared to the Si-NMP samples. This indicates that a thinner and ostensibly more passivating SEI has evolved in the Si-Pitch system.

To further probe the solid-phase SEI, XPS was conducted on a separate portion of the recovered Si-NMP and Si-Pitch electrodes that had

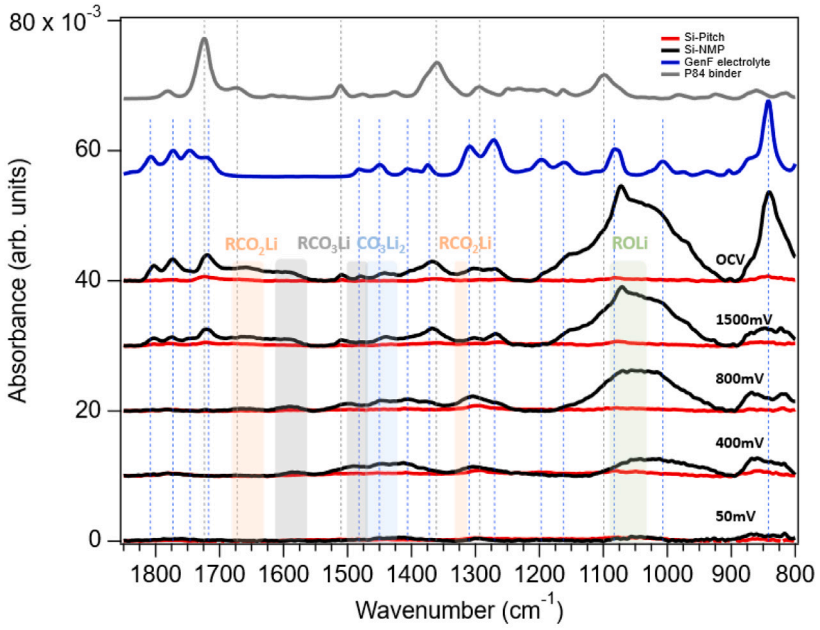

Fig. 3. FTIR spectra of Si-Pitch (red) and Si-NMP (black) electrodes recovered from half coin cells following 180 h voltage hold at targeted reduction (lithiation) potentials. Spectra of P84 binder (gray) and GenF-10 electrolyte (blue), with vertical dashed lines at significant peaks, are also included for reference.

undergone FTIR analysis. XPS spectra of the Si-Pitch samples indicate the evolution of full SEI surface coverage by 400 mV (Fig. 4). This is evidenced by the reduction in the total Si 2p signal to near-baseline. In contrast, the Si-NMP sample shows high Si 2p signal, indicative of surface-exposed Si. Not until 50 mV – the maximum lithiating potential evaluated in this study – does the Si 2p signal disappear. Taken together and from a simplistic perspective, these FTIR and XPS results support the notion that less Si surface is available and that there are fewer reactive bare Si sites in the Si-Pitch sample, such that passivation by full SEI coverage is achieved at higher potentials.

Further support for this mechanism is evidenced in the Si oxidation behavior with lithiation. Specifically, the presence of pitch is found to prevent oxidation of the Si during SEI growth. For the baseline Si-NMP sample, both the Si 2p and O 1s spectra indicate oxidation of the Si surface to SiO_x and SiO_2 prior to full SEI coverage. At OCV, the Si-NMP sample shows a distinct Si^0 peak at ≈100 eV and a broader SiO_x/SiO_2 peak between ≈102–105 eV. With increasing lithiation state (i.e., lower half cell potential) a shift of the predominant peak to higher binding energies is observed for the Si-NMP sample. This implies oxidation of Si^0 to SiO_x (≈101–103 eV) [30] before the Si 2p signal is masked by complete SEI coverage. Additionally, the Si-NMP sample appears to react with labile F species, which are likely evolved from the $LiPF_6$ electrolyte salt, at high potentials to form substantial quantities of SiO_xF_y. Such behavior is notably absent for the Si-Pitch sample: With increasingly reducing potentials, the initial quantity of SiO_x present at OCV is rapidly reacted or masked; the Si 2p signal is reduced in intensity but displays no observable binding energy shift and there is no evolution of SiO_xF_y. Deconvolution of the primary Si 2p peak at ≈100 eV implies a predominance of the Si^0 state in Si-Pitch at all states of lithiation, although the Si signal is largely masked by SEI at potentials < 1500 mV.

Notably, the Si-NMP sample also shows strong evidence of sample charging, which occurs in the absence of mobile Li to balance charge during the XPS measurement. In Fig. 4, this is manifest as the Si 2p spectral peak at ≈108 eV; by the presence of double peaks in the O1s spectrum between ≈534–537 eV for the higher cell potentials, i.e., OCV and 1500 mV; by the presence of broad double-peaks in the C1s spectra between ≈286–289 eV; and by the broad shoulder in the F1s spectra between ≈688–692 eV. The emergence of double-peaks and broad higher-binding-energy "echoes" of the dominant signals in these regions suggests that the Si-NMP sample consists of two disconnected particle environments, one of which experiences charging during analysis and the other of which does not. This charging behavior also implies that the Si-NMP sample is significantly electronically resistive to the depth of the XPS measurement (≈5–10 nm). At more highly lithiating potentials, evidence of charging is largely absent. This indicates that either the Si-NMP sample has become sufficiently electronically conductive (perhaps due to Si expansion strengthening contact with the surrounding carbon-binder network) or there is sufficient mobile Li to balance the charge. The fact that the Si-Pitch sample does not show charging behavior across all analyzed potentials indicates a lower electronic resistivity relative to the Si-NMP sample.

The solid-phase analysis presented in Figs. 3 and 4 provides evidence that the pitch-carbon coating serves to limit exposure of the native nano-Si to electrolyte, thereby limiting adverse electrolyte reduction processes that produce highly resistive SEI and concurrently minimizing oxidation of the underlying Si. FTIR and XPS results both imply that the Si-Pitch material experiences an "earlier" (i.e., higher-potential) grow-in of the SEI relative to Si-NMP, which could be the result of a lesser amount of exposed Si requiring passivation and could thereby result in the observed electrochemical performance improvements.

However, while this physicochemical barrier mode of pitch activity is a temptingly simple explanation, additional features of Fig. 4 necessitate a more complex interpretation. Beyond charging considerations, it is evident from the XPS spectra that the SEI composition of Si-Pitch is distinct from that of Si-NMP. For example, the F1s spectra indicates a predominance of LiF at the Si-NMP surface at all potentials analyzed, whereas the Si-Pitch samples show reduced LiF signal, on the same order of intensity of residual $LiPF_6$ salt (which is observed for both materials even following DMC rinsing). This disparity is most pronounced at the lithiating potential of 50 mV, where a dramatically lower signal from LiF is observed on the Si-Pitch surface relative to the Si-NMP surface. If the quantity of residual $LiPF_6$ salt is presumed to be relatively equivalent between the two samples, the P 2p spectra also imply a greater predominance of Li_3PO_4 and $Li_xPF_yO_z$-type species on the Si-NMP sample. Further, the O1s spectra reveals a Li_2CO_3-rich SEI at moderate potentials of 800 and 400 mV, whereas Li_2CO_3 is

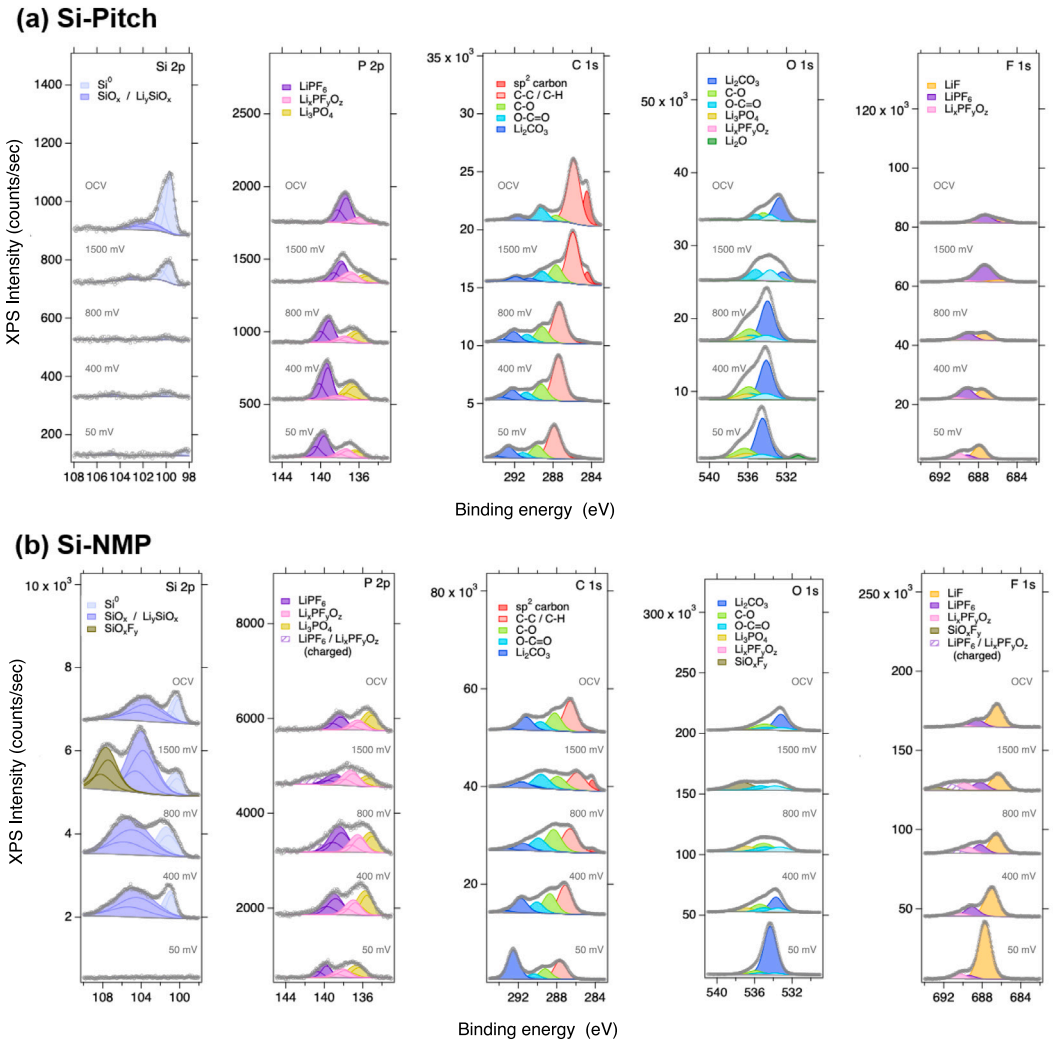

Fig. 4. XPS spectra and associated peak deconvolution with species assignments for Si-Pitch and Si-NMP samples following a 180 h voltage hold at each indicated potential. Spectra are each labeled with the value of their respective voltage-hold potential.

notably absent from the Si-NMP sample at 800 mV and only minorly present at 400 mV. Both Figs. 3 and 4 reveal a clear compositional distinction in the SEI evolved on these two Si composites across all potentials, suggesting that a more detailed explanation for the pitch-carbon coating's role in promoting improved nano-Si performance is warranted.

3.3. Pitch carbon promotes a more-favorable SEI

To pursue a more robust evaluation of the impacts of pitch-carbon on nano-Si performance, a multi-phase approach has been developed to probe solid, semi-volatile, and gaseous species compositions complementarily. Recent work [42] has emphasized the importance of such a multi-phase approach to understanding the inherently complex and convoluted network of three-phase reactions in Li-ion battery systems. In the present study, the solid-phase analysis of SEI products (Figs. 3 and 4) yields an "end point" of reactive/decomposition pathways. Qualitative and semi-quantitative analysis of volatile liquids and gaseous products can complement these results by providing additional insight into the mechanistic pathways underlying the observed SEI production. Specifically, pairing XPS and FTIR data (solid phase) with headspace (HS)-SPME GC–MS results (concentrated semi-volatile phase) and GC-FID signals (gaseous phase) for both Si-NMP and Si-Pitch informs a holistic view of the specific contribution of the pitch coating to Si surface passivation and associated performance improvements. As will be discussed, the present multi-phase data strongly supports the notion that the pitch coating drives the formation of an SEI that is compositionally distinct through (1) altering the role and functionality the fluoroethylene carbonate (FEC) additive by stabilizing radical intermediates and suppressing linear carbonate transesterification; and (2) altering the favorability of competitive reaction pathways.

3.3.1. Pitch as a "substitute" for FEC

In Si-containing systems, LiF evolution in the solid phase has been strongly correlated with FEC reduction [17,28,53] (although LiF has also been observed as an EC reduction product in a graphite system containing no FEC or linear carbonates [53]). A broadly reported FEC reduction pathway occurs according to Scheme 1 [18,34,53,54].

While the validity of the precise mechanistic pathway for FEC reduction has been challenged [9,55], there is broad consensus that reduction of FEC results in production of LiF, and that FEC is the predominant contributor to LiF formation in FEC-containing Si systems [18,34,53,54]. It is therefore reasonable to presume that, for systems where electrolyte and cell fabrication conditions are held constant, the generation of LiF may be taken as a qualitative indicator of the relative favorability of FEC reduction. The deconvoluted F1s signals in Fig. 4 and quantified ratios in Table 2 show that the surface of the Si-NMP sample is more significantly dominated by LiF at all hold potentials relative to the

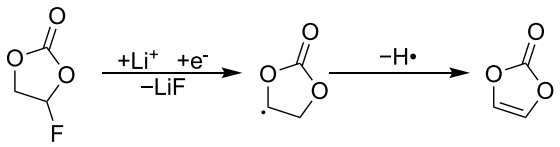

Scheme 1. Reduction pathway of fluoroethylene carbonate (FEC) as reported broadly in literature; see Refs. [18,34,53,54].

Table 2
Selected phase fractions and phase fraction ratios associated with SEI evolved on Si-NMP and Si-Pitch at each hold potential.

Sample	Hold potential (mV)	Phase fractions		
		LiF(%)	Li_2CO_3 (%)	LiF (%) / Li_2CO_3 (%)
Si-NMP	OCV	16.15	25.50	0.63
Si-Pitch	OCV	5.01	13.68	0.37
Si-NMP	1500	13.81	2.58	5.36
Si-Pitch	1500	3.31	7.17	0.46
Si-NMP	800	12.57	6.96	1.81
Si-Pitch	800	8.58	28.79	0.30
Si-NMP	400	17.84	20.92	0.85
Si-Pitch	400	10.03	25.77	0.39
Si-NMP	50	29.44	48.37	0.61
Si-Pitch	50	14.39	29.05	0.50

Si-Pitch sample (e.g., phase fraction of 13.81% LiF for Si-NMP versus phase fraction of 3.31% for Si-Pitch at 1500 mV).

Consistent with the concepts discussed in Section 3.2, the reduced active Si surface area in the pitch-coated sample is anticipated to inherently reduce the free electron density available to react with FEC and drive reduction. In absolute terms, this would suggest less total reduction of FEC for a Si anode composite with less surface-exposed Si. However, such interpretation does not account for the observed shift in speciation, and the *relatively* lower proportion of LiF observed as compared to other detected surface moieties such as $Li_xPF_yO_z$ and Li_2CO_3. For example, Table 2 and Table S2 show that at all potentials, Si-Pitch has significantly less LiF as compared to Li_2CO_3. This difference is more pronounced at higher hold potentials. For example, at 1500 mV, the ratio of LiF/Li_2CO_3 on the electrode surface is nearly 12 times greater for Si-NMP as compared to Si-Pitch. This indicates that FEC "acts differently" in the Si-Pitch sample relative to the Si-NMP material, and in particular, the decomposition of FEC appears to be diminished in the presence of pitch.

If the LiF production is defavored by the pitch coating, then the presence of reactants and products associated with the LiF decomposition pathway should also be impacted. As shown in Scheme 1, vinylene carbonate (VC) is a proposed mechanistic intermediate of FEC reduction [18,34,53], and VC signals have repeatedly been observed experimentally [18,34]. In the present analysis, SPME was conducted on separator samples recovered from coin cells following voltage hold at each potential of interest. These SPME results serve as a proxy for the semi-volatile composition of the liquid phase and can be applied to evaluate the evolution of VC in both Si-Pitch and Si-NMP samples. Such an approach has previously been employed to characterize the headspace composition of a variety of cells with high fidelity [38]. While robust quantification of headspace components through SPME is feasible, it requires preparation of well-defined volatile standards with known analyte compositions, which is significantly time-intensive and was not undertaken for the present study. However, with careful consideration for consistency in cell preparation and disassembly procedures and fiber adsorption/desorption times, the SPME-GC-MS signal (Figure S2) is a linear function of concentration in the headspace — and therefore also in the liquid phase, if equilibrium vapor pressure is assumed.

Fig. 5 illustrates the integrated intensity of VC signals (with VC identity confirmed using National Institute of Standards and Technology (NIST) database matching of the MS spectra) as a function of voltage-hold potential. There is no clear monotonic trend of VC intensity with potential for either sample; however, there is notably lower VC content for all Si-Pitch samples relative to Si-NMP samples at each voltage-hold potential. Interestingly, the lowest VC content for the Si-NMP sample is observed at the most reducing potential (50 mV), which also aligns with the highest observed phase fraction of LiF (Table 2).

It is notable that VC is observed in this system at all potentials — including OCV. This result suggests that VC production occurs even in the absence of applied electrochemical potential. The fundamental mechanisms proposed in literature to describe FEC reactivity remain under debate, with some reports suggesting pathways that entirely preclude the direct evolution of VC as an intermediate product in the liquid phase [9,55]. The mechanism of FEC reduction shown in Scheme 1 remains contested in the current literature, largely because it requires the presence of reduced carbonate species to serve as the bases attacking FEC. These reactants include lithium alkoxide species (LiOR, e.g. LiEMC, dilithium ethylene dicarbonate (LiEDC), etc.) which are primarily derived from reduction of linear carbonates [16,57]. The nominal equilibrium reduction potential of EMC is predicted by density functional theory to be substantially lower than that of either FEC or EC (0.52 V vs Li^+/Li for EMC reduction; 0.87 V for FEC reduction; and 0.67 V for EC reduction have been reported for a simulated GenF-10 electrolyte) [42]. Given the high thermodynamic reduction potential of FEC, these reduced carbonate species should not ostensibly be present. While VC may be formed through alternative pathways – for example, through decomposition of linear carbonates such as EMC [42] – the nominal reduction potential of these linear carbonates is even lower than that of FEC. Thus, it has been argued that VC should not be an expected product from FEC reduction [9,55]. However, the clear detection of VC (Fig. 5) concurrent with the production of LiF (Fig. 4) provides experimental support for the notion that other reduced species must be present at potentials as high as 1500 mV to drive the observed electrochemical reduction of FEC to VC. As shown in Fig. 5, VC production is clearly at least in part potential-driven, with signals at each measured reduction potential exceeding that attributable to pure chemical reactivity at OCV.

In situ gas-phase signals further bolster this conclusion. Specifically, carbon monoxide (CO) is produced concurrently with LiOR during carbonate reduction (Scheme 2), and as such, CO may be employed as an indicator of LiOR species generation [56]. Fig. 6a reports the concentration of CO evolved from Si-Pitch and Si-NMP half cells after 180 h voltage hold at each of three potentials. It is immediately evident that substantially higher intensity of CO (intensity linearly proportional to concentration) is observed for the Si-NMP sample across all potentials, but particularly at and below 800 mV. For the Si-Pitch sample, CO concentrations decrease consistently between 1500 and 50 mV.

Taken together, the observed presence of LiOR and associated reaction products, such as CO, offers an interesting perspective to consider the performance benefits imparted by pitch-carbon coating on nano-Si. When present in the electrolyte, LiOR species are known to catalyze not only the reduction of FEC to VC and LiF, but also the pathway of transesterification of the linear carbonates. In the transesterification process, the alkoxide group (RO−) on the native linear carbonate (EMC) is (reversibly) substituted by the alkoxide group of the reduced LiOR species to form, for example, DMC. Transesterification has been broadly observed experimentally [16,36,38,56,57] and several thermodynamically favorable pathways describing this phenomenon have recently been reported [42]. Left unchecked, transesterification can lead to reduced cell performance, including sudden cell failure [16].

Several reports have noted the critical role that additives such as VC [36,38] and FEC [16,38] can play in suppressing transesterification. It may be intuitively presumed that such an effect is achieved through preferential reduction of the additive (rather than the linear carbonate), such that LiOR production would be avoided. However, it has been demonstrated that instead, these additives function primarily through

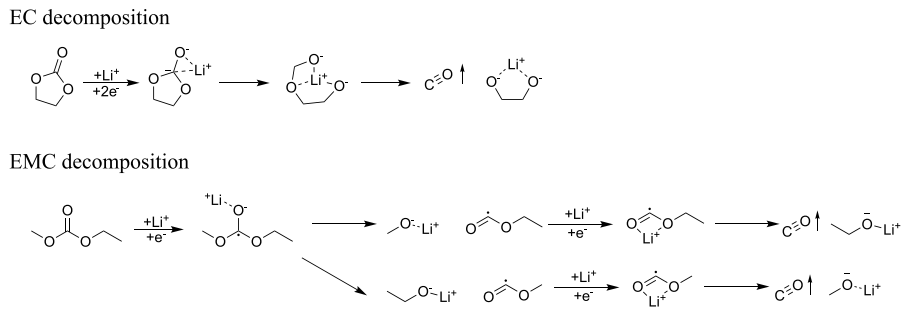

Scheme 2. Proposed mechanisms for (a) cyclic carbonate (EC) and (b) linear carbonate (EMC) decomposition to concurrently form LiOR and CO; see Refs. [42,56].

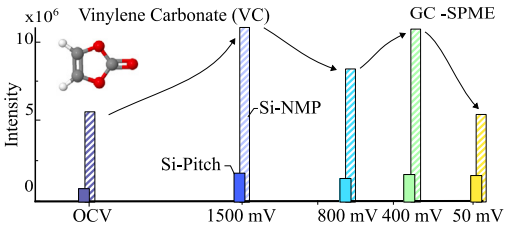

Fig. 5. Variation of vinylene carbonate (VC) intensity measured via GC-SPME for Si-Pitch (solid) and Si-NMP (dashed) samples across multiple reduction potentials.

a method of lithium alkoxide trapping, whereby LiOR is still produced, but the additive preferentially reacts with and consumes LiOR rather than LiOR persisting in solution and remaining available to drive transesterification [16,33,56,58].

For FEC in particular, the mechanism of alkoxide trapping is reported to occur according to the reaction given in Scheme 3, which produces alkoxide-substituted FEC products [16]. Such products occur in trace concentrations relative to the bulk electrolyte composition, and thus are rarely reported. However, their presence has been confirmed in the present work via SPME-GC-MS analysis. As shown in Figure S7, SPME-GC-MS of the volatile headspace of a separator recovered from Si-Pitch electrodes cycled in GenF-10 reveals two compounds with molar masses of 118 and 132 g mol^{-1}. These species are unindexed in the NIST database, but exhibit mass selective detector (MSD) chromatograms precisely consistent with those detected [16] and have been assigned as alkoxide-substituted FEC products, consistent with the reaction given in Scheme 3.

The extent of alkoxide trapping is dependent on both the availability of the "trapping" species and the relative kinetics of alkoxide generation vs. alkoxide trapping [56]. For the Si-NMP sample, FEC is the only viable trapping solvent. However, as has been mentioned, Si-Pitch also contains substantial sp^2 carbon functionality that may similarly facilitate alkoxide trapping, thereby mitigating transesterification. Previously, a C_4H_6 (butadiene) additive was reported to offer better LiOR scavenging properties than VC; this has been attributed to the resonance stabilization of negative charge evolved during the nucleophilic attack of LiOR [56]. The pitch-carbon coating, with its extended conjugated carbon network, would therefore be expected to substantially enhance such resonance stabilization and thereby favor LiOR trapping, as proposed in Scheme 4.

It should be noted that multiple distinct species in the cell system are known to facilitate LiOR consumption, including FEC [16,38], VC [36,38], and CO_2 [33,56,58] – and, we propose, the pitch-carbon coating as well. While it is probable that all of these species contribute to the reactive consumption of LiOR to some degree, factors such as FEC content were intentionally maintained consistent between samples, and all other controllable sources of variation between the samples were minimized such that major changes in signal intensity can be attributed to the presence (or absence) of pitch. Since (1) previous findings suggest that resonance-stabilized conjugated species preferentially scavenge LiOR more than species with a single reactive double-bond [56] and (2) XPS results in Fig. 4 and Table 2 indicate a relatively lower production of LiF (i.e., lower extent of FEC reduction) in Si-Pitch samples, we conclude that *the pitch-carbon coating is the predominant species reactively consuming LiOR in the Si-pitch system*. The FTIR data in Fig. 3 provide further support for this hypothesis. Specifically, the Si-Pitch sample shows significantly lower absorption around 1070 cm^{-1} at all hold potentials, which is the spectral region associated with the C-O vibration stretch of an alkoxy moiety, i.e., LiOR [33,52].

Thus, there is robust multi-phase evidence indicating that pitch-carbon coating is altering the "typical" FEC functionality in the nano-Si system. XPS results (Fig. 4 and Table 2) suggest that the typical decomposition pathway of FEC is defavored, resulting in both reduced VC signals (detected by SPME-GC-MS) and relatively lower LiF content in the solid phase. This carbon network is also hypothesized to facilitate more alkoxide scavenging relative to FEC for Si-Pitch versus Si-NMP samples, across all potentials.

These findings all point to the conclusion that FEC plays a different, and perhaps lesser, role in stabilizing the SEI in Si-Pitch, with the pitch-carbon network instead assuming much of the beneficial functionality typically ascribed to FEC. This implies that using FEC as an additive may be less critical for Si-Pitch electrodes as compared to other Si-based electrode systems. Such a conclusion has been qualitatively borne out in recent experimental studies by our group of various nano-Si materials in novel electrolyte systems (data as yet unpublished), whereby FEC addition is found to negligibly improve cycling performance for the Si-Pitch samples, whereas FEC drastically improves the cycling stability of nano-Si materials with alternative surface coatings. Reduced FEC consumption in the Si-Pitch sample implies that the FEC additive will be retained in the electrolyte for longer, where it may serve additional beneficial roles such as preventing $LiPF_6$ decomposition and preventing catastrophic failure associated with FEC depletion that has been reported for Si-based cells [17].

3.3.2. Pitch alters reaction competitive favorability

Beyond merely subsuming some of the functionality of FEC, the present data suggests that the pitch-carbon coating is likely altering the relative favorability of competitive SEI-forming reactions, resulting in the production of a "better" SEI. While SEI-generating reaction pathways have traditionally (and reasonably) been probed primarily through solid-phase characterization techniques, gas-phase analysis is a powerful complementary approach to probe reaction identity and extent. An example of this complementarity has already been discussed (Fig. 6a, whereby CO may be used as a proxy for detection of LiOR in the liquid phase, and by extension, the transesterification reaction pathway).

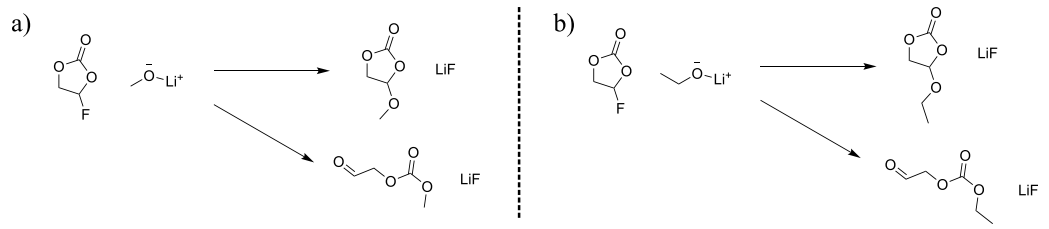

Scheme 3. Proposed mechanisms for FEC reaction with LiOR to form alkoxide-substituted product; see Refs. [16,42].

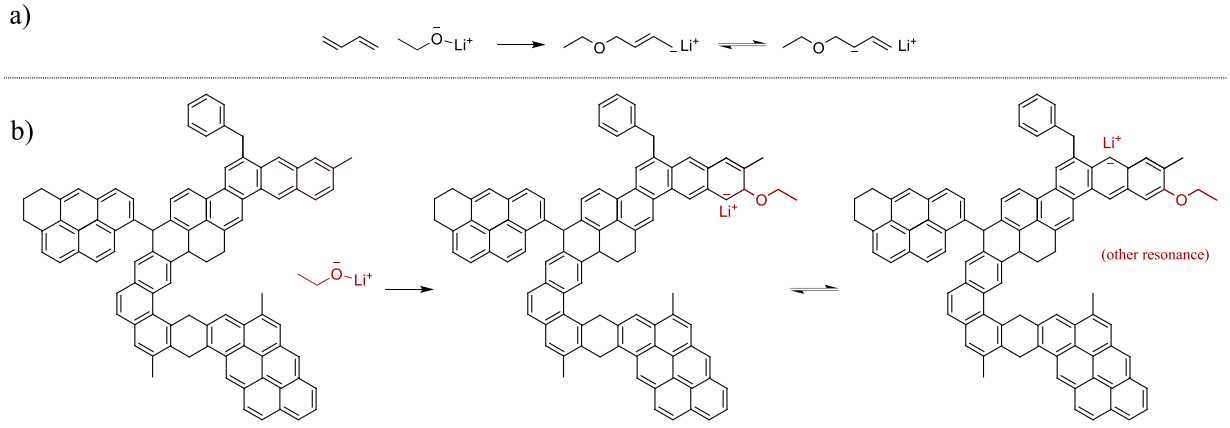

Scheme 4. Alkoxide trapping mechanism facilitated by resonance stabilization: (a) Previously proposed mechanism for alkoxide scavenging by butadiene, according to Ref. [56]; (b) Suggested mechanism for alkoxide scavenging by pitch-carbon supported by the present results.

In this study, we have utilized an in situ gas analysis approach in which cells are fabricated with realistic (rather than mesh or model-system) electrodes in a coin-cell-type format, which maximizes direct translational comparison with electrochemical and ex situ data from traditional coin cells. Our coupled GC-MS-FID system facilitates a broad scope of analyte detection, with GC separation facilitating distinct analyte qualitative identification and MS or FID detection providing semi-quantitative concentration information, i.e., intensity is linearly proportional to concentration. The present approach enables robust identification and quantification of relative concentrations of gaseous products in an in situ format, while minimizing artificial disruptions to realistic cell operation induced by sampling. It is worth noting that in the present study, each cell was brought immediately to the hold-potential of interest and a sample was extracted after a 180 h hold at that potential. This notably results in distinctly different data than if each potential-point had been measured consecutively, e.g., through techniques such as differential electrochemical mass spectrometry (DEMS).

For Si systems in particular, gas evolution and gas-phase composition have been recognized as both critical indicators and influencers of reactivity. Fig. 6 shows a complete set of potential-resolved gas-phase data for all major detected gaseous species observed in Si-Pitch and Si-NMP cells after a 180 h voltage hold at each of the indicated potentials. The identity and relative quantities of gases evolved from Si-containing systems across a range of thermodynamically relevant potentials offers insight into competitive reaction pathways. These pathways may be complex, convoluted, and can involve multiple plausible pathways producing the same gaseous species [42]. Even in the absence of applied potential, the Si surface chemistry, including the Si termination, is known to influence the nature of evolved gases [13]. Further, the presence of gases that are typical products of electrolyte reduction processes during SEI formation directly influence the favorability of additional SEI-forming reactions and the resulting solid-phase products [59]. Given such inherent convolution, specific attribution of each species at each potential to an explicit pathway (or pathways) based solely on (electro)chemical intuition is not feasible. Even in light of the robust multi-phase complementary analysis reported herein, it is similarly implausible to attempt specific mechanistic deconvolution through precise experimental detection of all complementary evolved species for a given pathway, since there are hundreds of relevant species and reactive intermediates spanning all three phases. Instead, several prominent trends that emerge from this gas-phase data will be discussed and tied to solid- and volatile-liquid-phase data to further determine the role of pitch-carbon coating in improving the performance and (electro)chemical stability of nano-Si.

First, a comparison between the gas-phase signatures of Si-Pitch and Si-NMP reveals that Si-Pitch shows *higher* concentrations of all major hydrocarbon gases (CH_4, C_2H_4, C_2H_6) relative to Si-NMP at 1500 and 50 mV (Fig. 6c, e, f). Conversely, at 800 mV, Si-Pitch shows *lower* concentrations of CH_4 and C_2H_6 relative to Si-NMP. Gas-phase analysis of Si-Pitch and Si-NMP soaked in GenF-10 in the absence of an applied potential has recently suggested that Si-Pitch in both powder and electrode configurations reacts to evolve higher concentrations of CH_4 and C_2H_6 gas relative to Si-NMP [27]. The gas-phase signatures of Si-Pitch and Si-NMP at 1500 mV are consistent with this previous observation for CH_4 and C_2H_6 evolution at OCV [27] (Fig. 6c and Fig. 6f, respectively). At more reducing potentials, however, Si-NMP shows increased electrochemical reactivity over Si-Pitch, with higher relative production of alkane gases observed in the Si-NMP sample at 800 mV. The generation of CH_4 and C_2H_6 has been largely attributed to the reductive decomposition of linear alkyl carbonates [53,60] (although isotopic labeling in a comparable baseline electrolyte system implies that reduction of the cyclic carbonate may also contribute to alkane gas production to a lesser degree [40]). This data is consistent with the suppression of linear carbonate decomposition and associated transesterification reactions, as put forward in Section 3.3.1.

The gas evolution behavior of the two Si materials when held at 1500 mV differs from that observed during soaking experiments, however, with regards to the relative intensity of C_2H_4 evolved. Specifically, a higher intensity of C_2H_4 is observed for the Si-Pitch sample as compared to the Si-NMP sample at 1500 and 800 mV, despite the fact that Si-Pitch is known to produce less C_2H_4 as compared to Si-NMP when

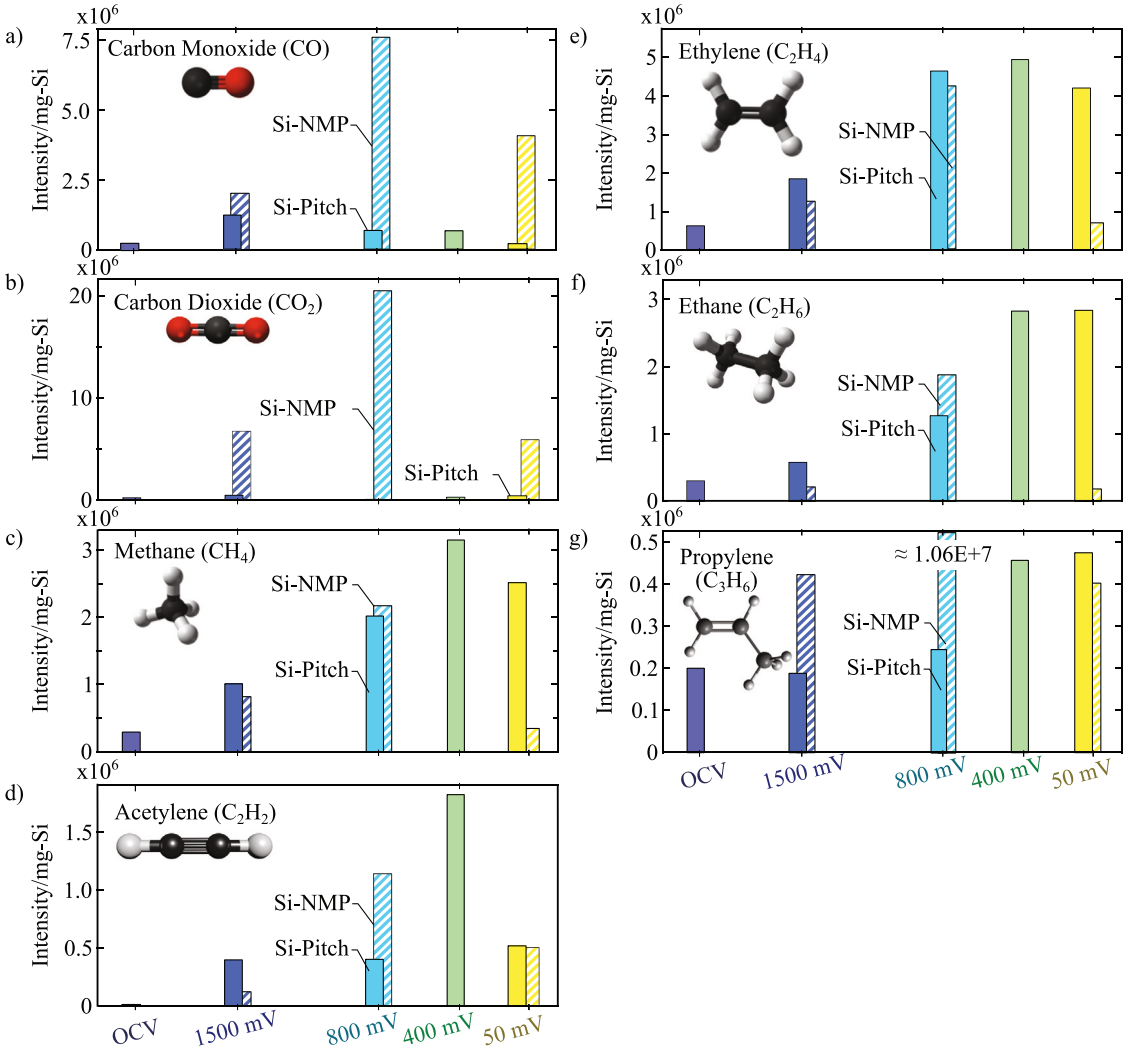

Fig. 6. Voltage-resolved evolution of seven gaseous species detected in Si-Pitch (solid) and Si-NMP (dashed) samples via GC-FID.

soaked in GenF-10 [27]. Isotopic labeling results [40] and extensive previous literature reports have suggested that C_2H_4 is evolved nearly exclusively from EC degradation. Given that the gas-phase signals are reported as intensities rather than absolute values, a higher observed intensity of C_2H_4 in the Si-Pitch sample at higher potentials could indicate either: (1) Si-Pitch is driving selective degradation of EC, or (2) other pathways associated with Si-NMP (electro)chemical reactivity are dominant at these potentials, resulting in lower concentration of C_2H_4 relative to total gas produced. Analysis of Fig. 6 (and Figure S8, where the data in Fig. 6 is replotted in an alternative form for ease of comparison and interpretation) lends weight to this latter interpretation. In particular, substantially higher CO and CO_2 generation is observed for Si-NMP relative to Si-Pitch at 1500 mV and 800 mV, and values of C_2H_2 and C_3H_6 are also elevated for the Si-NMP sample at these potentials. Moles-based analysis – which requires additional robust measurements of pressure and volume at every system state – is under development to strengthen direct comparisons of the gas-phase signatures between these materials.

A second critical result is the potential-dependent non-monotonic trend in species intensity observed for nearly all of the gaseous products detected in the Si-Pitch system (Fig. 6). Notable exceptions are C_2H_6 and C_3H_6, each of which increase in concentration from OCV to 400 mV and stabilize at 400 mV. For Si-NMP at the three lithiating potentials measured, the same non-monotonic trend is observed for all species: concentrations of each measured species increase between 1500 and 800 mV, and then decrease between 800 and 50 mV (Fig. 6).

Fig. 6 shows that the majority of hydrocarbon species detected in the Si-Pitch sample reach a maximum concentration value at 400 mV, including CH_4, C_2H_4, C_2H_6, C_3H_6, and C_2H_2. The 400 mV potential point was selected in this work to be the voltage at which predominant SEI-forming reactions (i.e., thermodynamically predicted electrochemical reduction of both FEC and EC) should be "turned on", but lithiation of the Si should not yet be occurring. Of these five gaseous species, C_2H_6 and C_3H_6 remain virtually constant in concentration between 400 and 50 mV, while CH_4 and C_2H_4 show a slight decrease in concentration and C_2H_2 shows a substantial decrease in concentration, to a value comparable to that observed at 1500 and 800 mV. From an intensity-agnostic point-of-view, the relative rates of potential-dependent change are nearly identical for C_2H_6 and C_3H_6, indicating that these two species are either: (1) formed from a shared set of reactants through the same mechanistic pathway (a precise mechanism to describe this has not been suggested, to our knowledge); (2) evolved from distinct reactants that are produced in complementary or stoichiometrically related pathways; (3) formed through distinct pathways with similar thermodynamic favorability at each given potential.

The behavior of the oxide gases (CO and CO_2; Fig. 6 a, b) is perhaps the most erratic for both the Si-Pitch and Si-NMP samples, with substantial CO and CO_2 generation observed at 1500 mV — above the electrochemical reduction potential for most reported reactions. In fact, nearly all gaseous species observed (except for C_3H_6) are present in elevated concentrations at 1500 mV, relative to what may be attributed

to the pure chemical reactivity "baseline" measured at OCV. Reactivity at high potentials is typically attributed to the reduction of trace contaminants, including HF, alcohols, or water present in the system [13]. CO_2 production resulting from EC hydrolysis has been reported at potentials around 1500 mV [56], which is also the electrochemical potential regime in which formation of LiF may occur in the presence of $LiPF_6$ hydrolysis [49]. Additional discussion on this point is taken up in Section 4.1.

Taken as a whole, Fig. 6 implies that the enhanced electrochemical stability observed for nano-Si in the presence of a pitch-carbon coating is not associated merely with suppression of *all* gas-generating reactions. Rather, the distinct shift in the balance of *which* gaseous species are observed at each measured potential between Si-NMP and Si-Pitch implies that *the pitch coating is altering the favorability of various competing reactive pathways*. Surface energy differences between the materials, the relative (un)favorability of FEC reduction given the competitive contributions of pitch, and the varying signatures associated with pure chemical reactivity of Si-NMP vs. Si-Pitch are all expected to contribute to determining which pathway(s) dominate at each potential to produce the resulting gas-phase species.

Finally, given the 180 h hold period at each measured potential prior to sampling, gas consumption may be a contributing factor to the observed non-monotonic behavior with respect to potential. Gas consumption beyond that attributable to side-reactivity [56] or gas solubility [61,62] has been observed and reported in a variety of cell systems, particularly over longer storage periods [61]. Such behavior indicates that these gaseous species may be serving as reactants as well as products in SEI-forming reactions.

Mechanistic pathways describing gas consumption are generally less studied and are less well understood as compared to pathways driving gas production. Previous reports have noted and emphasized CO_2 consumption in both graphite and Si anode systems [33,56]. Carbon dioxide consumption is believed to facilitate more favorable SEI evolution by suppressing transesterification reactions [56] and the resulting production of more cross-linked PEO-type polymeric species [33]. This mode of improvement is consistent with behavior of the Si-Pitch sample discussed in the preceding sections. Presuming that the conjugated pitch network subsumes the alkoxide-scavenging role otherwise taken on by CO_2, Si-Pitch would be expected to exhibit less CO_2 consumption relative to Si-NMP. The present data support such conclusion: As shown in Fig. 6b, the CO_2 concentration detected after a 180 h hold at 50 mV is 74.2% higher than that measured after a 180 h hold at 800 mV for the Si-Pitch sample, whereas the CO_2 concentration at 50 mV is 70.8% lower than that at 800 mV for the Si-NMP sample under the same hold-time conditions. A higher degree of CO_2 consumption in the Si-NMP sample between 800 and 50 mV could plausibly be contributing to this observed trend. In other words, in Si-NMP, some CO_2 is consumed by alkoxide scavenging reactions, whereas in the presence of pitch, the conjugated carbon network of the pitch subsumes the alkoxide scavenging role and is acting like an additive to scavenge LiOR, similar to how CO_2 may be used as an additive [56]. There is also support for such conclusion in the solid-phase data: As reported in Section 2.3, the Si-NMP sample shows a higher concentration of LiF and a relative suppression of Li_2CO_3 relative to Si-Pitch at all potentials (LiF/Li_2CO_3 for Si-NMP < LiF/Li_2CO_3 for Si-Pitch; Fig. 4 and Table 2). This is consistent with behavior previously observed for a Si thin-film half-cell system doped with an excess of CO_2 [33], which by thermodynamic arguments would suggest CO_2 consumptive pathways.

For several of the other gases exhibiting non-monotonic responses, including C_2H_4 and CO, plausible consumption pathways to solid-phase products have been proposed [61]. However, other species such as the alkane gases (CH_4 and C_2H_6) are not reported to be substantially consumed in traditional graphite systems [61], and to our knowledge, there are no reported mechanisms to describe the consumption of either these alkane gases or the other reported minor species such as C_2H_2, C_3H_6. The present results highlight the need for time-resolved measurements to complement the present potential-resolved data to deconvolute gas consumption phenomena from the balance of competitive reaction pathways. Such experiments, in conjunction with a robust moles-based quantification approach and close integration with continuum-level modeling, are presently underway.

4. Additional considerations

Beyond the above-described hypotheses regarding the specific role of pitch carbon on the (electro)chemical reactivity of nano-Si, several additional considerations are critical to robustly understand the observed performance of the present system as well as other similar next-generation Si systems. Three such considerations are outlined below.

4.1. Considering the impact of trace water on SEI composition

In the present study, both Si-NMP and Si-Pitch samples show substantial reactivity at potentials above 1500 mV. As noted, the signals at 1500 mV are in excess of those observed at OCV. There are a select few reports of reductive pathways with thermodynamic potentials in this regime: Han et al. [9] suggest that lithium silicides may chemically react with electrolyte solvents to reduce both EC and FEC, and the electron density provided at 1500 mV might be sufficient to initiate such a reaction cascade. Jin et al. [20] report FEC and VC decomposition at potentials as high as 1300 mV vs. Li^+/Li for a system of Si nanowires, and it is plausible that that the pitch coating and/or NMP surface termination could provide a sufficient reduction in surface energy to lower the onset potential for this reaction and produce the signals observed at 1500 mV. Alternatively or additionally, previous work has suggested that by applying even a minimal electrochemical potential, Li-ions are driven to the anode, which will drag additional bound solvents and PF_6^- anions to the reactive Si surface. This may alter reaction kinetics and result in the higher total amount of gaseous products at 1500 mV relative to that evolved at OCV [13,50].

The role of water and trace impurities, which can never entirely be removed in a practical battery system, should not be ignored. In addition to the ppm-level quantities of water present in all commercial electrolytes, it has been suggested that 2–3 monolayers of strongly-bound "surface water" can persist on electrodes, even when such materials have been vacuum-dried above 300 °C [63]. Given the low volume of electrolyte used in a coin-cell configuration and the extremely high surface area of materials such as nano-Si, even monolayer presence of surface water may translate to non-negligible overall concentrations of water impurities in the electrolyte. As explored in detail in a previous study by Ha et al. [64], the presence of water strongly influences reactive pathways and can alter the composition and structure of the SEI. The transesterification reaction in particular – and the scavenging mechanism which suppresses it – both rely on the presence of lithium alkoxide species in the electrolyte. There is evidence in the present data that LiOR is evolved at potentials above the thermodynamic reduction potential of FEC, which is not predicted by theory and may imply the presence of trace water. Practically, eliminating trace water is unfeasible in any battery system, and it is particularly challenging to obtain highly dry electrodes without inducing damage to the binder [63]. Thus, rather than presuming a fully dry system, it is rather critical to understand and account for the impacts of trace water on SEI evolution and resulting cell performance.

4.2. Considering the role of Li metal

The present studies were conducted in half cells, which is a standard configuration for both electrochemical analysis and physicochemical characterization that is broadly employed across the battery research community. For gas analysis in particular, half cells offer a convenient approach to reducing the system complexity by removing so-called

"cross-talk" contributions from gas-generating reactions at the cathode. However, particularly when considering pathways for gas consumption, lithium may not be a truly inert component. Lithium has been repeatedly observed to *chemically* react with CO_2 [65], particularly in the presence of trace water, providing an additional pathway that contributes to apparent CO_2 consumption. In future studies, the influence of the Li counter-electrode on gas-phase signals will be probed by comparison with alternative counter-electrodes such as lithium iron phosphate.

4.3. Considering poly-VC evolution

In Fig. 5 and Section 3.3.1, VC was detected and its role as an indicator for the FEC reduction pathway was discussed. However, once formed, VC is known to be an unstable and reactive intermediate that is rapidly consumed until a stable SEI is developed [18]. Accumulation of VC in the electrolyte – as observed for the Si-NMP sample – is expected to occur with continuous FEC reduction. The *lower* concentration of VC observed for the Si-Pitch samples may therefore be a convolution of (1) a less favorable FEC reduction pathway producing less VC, and/or (2) enhancement of pathways that promote the reduction of VC to solid-phase species. In particular, VC is reported to undergo a radical reduction to produce polymeric "poly-VC"-type species [34], which have been repeatedly observed through solid-phase surface characterization and are often used to explain performance improvements achieved when employing VC as an electrolyte additive [18,20,34,66]. The production of LiF and VC is expected to occur in stoichiometric equivalency with the reduction of FEC (Scheme 1), whereas further reduction of VC to poly-VC is a catalytic process [34].

Poly-VC has been previously detected via FTIR in FEC-containing electrolyte systems [28], but was not observed in substantial quantity in either sample in the present work. This may be attributable to resolubilization of poly-VC in dimethyl carbonate (DMC) during the brief electrode rinse conducted prior to FTIR analysis, given that poly-VC is reportedly soluble in several other polar aprotic solvents [67]. VC-derived polymeric SEI species have been shown to consist of both cross-linked PEO- or poly-VC-type regions (Li-ion conducting) and aliphatic regions (electronically insulating) [20], with the branched structure ostensibly contributing enhanced mechanical properties and better accommodating volume expansion [18,20]. The pitch coating on the Si-Pitch sample consists of an extended sp^2-carbon-rich polycyclic aromatic hydrocarbon network [27,68], which may reasonably be expected to provide pi conjugation stabilization of the VC radical and promote the formation of a highly favorable poly-VC-rich SEI according to this mechanism. In fact, SEM imaging of the Si-Pitch electrode after formation cycling (see Supplementary Material) qualitatively suggests a pliant SEI; this is in contrast to previously collected SEM of Si-NMP following cycling, which shows visible cracking, suggesting an inflexible SEI [26]. Thus, the contribution of poly-VC to the observed enhancement of Si-Pitch performance relative to Si-NMP cannot be conclusively discounted. Further analysis is underway to deconvolute whether the lower VC signal in Si-Pitch relative to Si-NMP is exclusively due to less FEC reduction, or whether the pitch coating may also be favoring the evolution of a branched poly-VC-rich SEI with enhanced stabilization properties.

4.4. Considering the role of electro-active carbon

Throughout this study and in previous reports, carbonaceous coatings on Si have been considered primarily as surface-modifiers to the Si substrate. In this view, the benefit of such coating is entirely associated with protecting the Si core from adverse electrochemical reaction through the formation of a "better" SEI. It is typically presumed that the Si core contributes the entirety of the reversible electrochemical performance. However, there is evidence that the pitch-carbon may itself be electro-active, which is unsurprising given that carbon black materials are known to exhibit appreciable Li-ion storage capacity [69]. In our group's previous studies, we have shown that pitch-carbon only electrodes, analogous to those employed in this work, show nearly 450 mAh g^{-1}-carbon [70]. Further, Li storage has been demonstrated in 2-D layered covalent organic frameworks (COFs), which consist of a functional pi-electron system highly analogous to that of pitch carbon. In these 2-D COFs, the sp^2 carbon network is found to function similarly to a graphite electrode, promoting (de)lithiation through C-Li bond formation and concurrently producing an SEI-type passivating layer. Thus, it is likely that beyond the surface stability enhancements described herein, the pitch-carbon coating contributes an added benefit of supplemental electro-activity. This may further facilitate the observed performance benefits associated with Si-Pitch relative to alternative nano-Si materials.

5. Conclusion

In this study, we have taken a holistic multi-phase approach to elucidate how the introduction of a pitch-carbon coating onto nano-Si material leads to observed improvements in Si calendar life. The present data support two primary hypotheses, which we have explored in detail. First, the pitch-carbon is found to serve as a physicochemical barrier, reducing the inherently high surface area available for the nano-Si material to react with electrolyte. This concurrently prevents the oxidation of the Si to SiO_x and SiO_2 that is deleterious to anode performance [43]. Second, there is evidence that the pitch-carbon coating promotes the evolution of a more-favorable SEI. The pitch carbon subsumes substantial functionality typically associated with the FEC additive that is known to contribute to enhanced cell performance. Specifically, the pitch coating appears to facilitate alkoxide scavenging, which mitigates deleterious transesterification reactions. We anticipate that such behavior is facilitated through radical stabilization by the conjugated carbon network of the pitch-carbon. Further, there is strong evidence that the pitch carbon is shifting the favorability of various plausible competing reaction pathways for SEI growth through relative suppression of the FEC reduction pathway and modification of the Si surface energy. These mechanisms work synergistically so that the pitch coating reduces how much interfacial chemistry happens and simultaneously directs what chemistry does happen into forming a better SEI, earlier in the lithiation window. That dual action explains the improved passivation, lower parasitic currents, and improved cycling and calendar-aging performance of Si-Pitch versus Si-NMP. The mechanisms of performance improvement observed herein for Si-Pitch can be capitalized and expanded on to inform the rational design of improved nano-Si materials. To this end, a couple of recent examples show how nanoporous Si confined within doped carbon frameworks can maintain structural integrity, enhance electronic transport, and stabilize the SEI [71,72].

Our approach intentionally utilizes a suite of complementary diagnostic techniques to robustly evaluate the three-phase speciation developed in Si-containing Li cells. By studying the end-product evolution of complex (electro)chemical interfacial reactions in all phases, we can more robustly interpret the role of the Si surface coating on improved electrochemical performance. A complete understanding of the initial (formation) and continual evolution of the SEI, electrolyte degradation, and gaseous formation requires diagnostic techniques and approaches that study the solid, liquid, and gas phases present in Li-ion batteries. Future work includes full-cell validation with detailed interfacial characterization on both electrodes, building on our prior full-cell study [27]. As additional technologies are developed to realize "beyond Li" batteries, it is expected that multi-phase characterization approaches will become an increasingly essential complement to robust electrochemical analysis to rapidly identify and address deleterious chemical mechanisms.

Acronyms

	Definition
ATR	Attenuated total reflectance
DEMS	Differential electrochemical mass spectrometry
DMC	Dimethyl carbonate
EC	Ethylene carbonate
EMC	Ethyl methyl carbonate
FEC	Fluoroethylene carbonate
FID	Flame-ionization detector
FTIR	Fourier Transform Infrared Spectroscopy
GenF-10	1.2 M $LiPF_6$ in 3:7 wt:wt EC:EMC + 10 wt.% FEC
GC	Gas chromatography
GC–MS	Gas chromatography-mass spectrometry
HS	Headspace
ID	Inner diameter
LiEDC	Dilithium ethylene dicarbonate
LiOR	Lithium alkoxide species
MS	Mass spectrometer
MSD	Mass selective detector
NMP	N-methyl-2-pyrrolidone
NMR	Nuclear magnetic resonance
OCV	Open-circuit voltage
OD	Outer diameter
SEI	Solid-electrolyte interphase
SEM	Scanning electron microscopy
SPME	Solid-phase micro-extraction
SSRM	Scanning spreading resistance microscopy
ssNMR	Solid-state nuclear magnetic resonance
TEM	Transmission electron microscopy
VC	Vinylene carbonate
XPS	X-ray photoelectron spectroscopy

CRediT authorship contribution statement

Kae E. Fink: Writing – review & editing, Writing – original draft, Visualization, Validation, Supervision, Methodology, Investigation, Formal analysis, Conceptualization. **Peter J. Weddle:** Writing – review & editing, Writing – original draft, Visualization, Conceptualization. **Jack R. Palmer:** Writing – review & editing, Visualization, Investigation, Conceptualization. **Christof Zweifel:** Writing – review & editing, Investigation. **Glenn Teeter:** Writing – review & editing, Validation, Investigation, Formal analysis. **Ankit Verma:** Writing – review & editing, Writing – original draft, Visualization, Methodology, Formal analysis. **Shane Frisco:** Investigation. **Sang-Don Han:** Investigation, Conceptualization. **Maxwell C. Schulze:** Writing – review & editing, Resources, Investigation, Conceptualization. **G. Michael Carroll:** Writing – review & editing, Resources. **Andrew M. Colclasure:** Writing – review & editing, Methodology, Funding acquisition. **Nathan R. Neale:** Writing – review & editing, Supervision, Resources, Funding acquisition, Conceptualization. **Bertrand J. Tremolet de Villers:** Writing – review & editing, Writing – original draft, Visualization, Supervision, Investigation, Funding acquisition, Conceptualization.

Declaration of competing interest

The authors declare the following financial interests/personal relationships which may be considered as potential competing interests: Nathan R. Neale has patent #11,459,242 B2 - Stabilized Electrodes for Ion Batteries and Methods of Making the Same issued to Alliance for Sustainable Energy LLC. G. Michael Carroll has patent #11,459,242 B2 - Stabilized Electrodes for Ion Batteries and Methods of Making the Same issued to Alliance for Sustainable Energy LLC. Maxwell C. Schulze has patent #11,459,242 B2 - Stabilized Electrodes for Ion Batteries and Methods of Making the Same issued to Alliance for Sustainable Energy LLC. If there are other authors, they declare that they have no known competing financial interests or personal relationships that could have appeared to influence the work reported in this paper.

Acknowledgments

This research was supported by the U. S. Department of Energy, Vehicle Technologies Office (DOE-VTO) under the Silicon Consortium Project, directed by Nicolas Eidson, Carine Steinway, Thomas Do, and Brian Cunningham, and managed by Anthony Burrell. This work was also supported in part by the U.S. Department of Energy, Office of Science, Office of Workforce Development for Teachers and Scientists (WDTS) under the Science Undergraduate Laboratory Internships Program (SULI).

This work was authored by NREL under Contract No. DE-AC36-08GO28308. The views expressed in the article do not necessarily represent the views of the DOE or the US government. The US government and the publisher, by accepting the article for publication, acknowledge that the US government retains a nonexclusive, paid-up, irrevocable, worldwide license to publish or reproduce the published form of this work, or allow others to do so, for US government purposes.

Appendix A. Supplementary data

Supplementary material related to this article can be found online at https://doi.org/10.1016/j.nanoen.2025.111597.

Data availability

Data will be made available on request.

References

[1] M.N. Obrovac, V.L. Chevrier, Alloy negative electrodes for Li-ion batteries, Chem. Rev. 114 (23) (2014) 11444–11502.
[2] M.C. Schulze, F. Urias, N.S. Dutta, Z. Huey, J. Coyle, G. Teeter, R. Doeren, B.J. Tremolet de Villers, S.-D. Han, N.R. Neale, G.M. Carroll, Control of nanoparticle dispersion, SEI composition, and electrode morphology enables long cycle life in high silicon content nanoparticle-based composite anodes for lithium-ion batteries, J. Mater. Chem. A 11 (10) (2023b) 5257–5266.
[3] J.D. McBrayer, M.-T.F. Rodrigues, M.C. Schulze, D.P. Abraham, C.A. Apblett, I. Bloom, G.M. Carroll, A.M. Colclasure, C. Fang, K.L. Harrison, G. Liu, S.D. Minteer, N.R. Neale, G.M. Veith, C.S. Johnson, J.T. Vaughey, A.K. Burrell, B. Cunningham, Calendar aging of silicon-containing batteries, Nat. Energy 6 (9) (2021) 866–872.
[4] H. Wang, S.-H. Lu, X. Wang, S. Xia, H.B. Chew, A review of the multiscale mechanics of silicon electrodes in high-capacity lithium-ion batteries, J. Phys. D: Appl. Phys. 55 (6) (2021) 063001.
[5] M.T. McDowell, S.W. Lee, W.D. Nix, Y. Cui, 25th anniversary article: Understanding the lithiation of silicon and other alloying anodes for lithium-ion batteries, Adv. Mater. 25 (36) (2013) 4966–4985.
[6] X.H. Liu, L. Zhong, S. Huang, S.X. Mao, T. Zhu, J.Y. Huang, Size-dependent fracture of silicon nanoparticles during lithiation, ACS Nano 6 (2) (2012) 1522–1531.
[7] X.-H. Liu, H. Zheng, Z. Zhong, S. Huang, K. Karki, L.Q. Zhang, Y. Liu, A. Kushima, W.T. Liang, J.W. Wang, J.-H. Cho, E. Epstein, S.A. Dayeh, S.T. Picraux, T. Zhu, J. Li, J.P. Sullivan, J. Cumings, C. Wang, S.X. Mao, Z.Z. Ye, Z. Zhange, J.Y. Huang, Anisotropic swelling and fracture of silicon nanowires during lithiation, Nano Lett. 11 (8) (2011) 3312–3318.
[8] G.M. Veith, L. Baggetto, R.L. Sacci, R.R. Unocic, W.E. Tenhaeff, J.F. Browning, Direct measurement of the chemical reactivity of silicon electrodes with $LiPF_6$-based battery electrolytes, Chem. Commun. 50 (23) (2014) 3081–3084.
[9] B. Han, Y. Zhang, C. Liao, S.E. Trask, X. Li, R. Uppuluri, J.T. Vaughey, B. Key, F. Dogan, Probing the reactivity of the active material of a Li-ion silicon anode with common battery solvents, ACS Appl. Mater. Interf. 13 (24) (2021) 28017–28026.
[10] Y. Xu, K. Wood, J. Coyle, C. Engtrakul, G. Teeter, C. Stoldt, A. Burrell, A. Zakutayev, Chemistry of electrolyte reduction on lithium silicide, J. Phys. Chem. C 123 (21) (2019) 13219–13224.
[11] M. Salah, P. Murphy, C. Hall, C. Francis, R. Kerr, M. Fabretto, Pure silicon thin-film anodes for lithium-ion batteries: A review, J. Power Sources 414 (2019) 48–67.
[12] M. Wetjen, D. Pritzl, R. Jung, S. Solchenbach, R. Ghadimi, H.A. Gasteiger, Differentiating the degradation phenomena in silicon-graphite electrodes for lithium-ion batteries, J. Electrochem. Soc. 164 (12) (2017) A2840.
[13] C.L. Seitzinger, R.L. Sacci, J.E. Coyle, C.A. Apblett, K.A. Hays, R.R. Armstrong, A.M. Rogers, B.L. Armstrong, T.H. Bennet, N.R. Neale, G.M. Veith, Intrinsic chemical reactivity of silicon electrode materials: Gas evolution, Chem. Mater. 32 (7) (2020) 3199–3210.

[14] A.L. Michan, M. Leskes, C.P. Grey, Voltage dependent solid electrolyte interphase formation in silicon electrodes: Monitoring the formation of organic decomposition products, Chem. Mater. 28 (1) (2016a) 385–398.

[15] M. Gauthier, T.J. Carney, A. Grimaud, L. Giordano, N. Pour, H.-H. Chang, D.P. Fenning, S.F. Lux, O. Paschos, C. Bauer, F. Maglia, S. Lupart, P. Lamp, Y. Shao-Horn, Electrode–electrolyte interface in Li-ion batteries: Current understanding and new insights, J. Phys. Chem. Lett. 6 (22) (2015) 4653–4672.

[16] R. Petibon, V.L. Chevrier, C.P. Aiken, D.S. Hall, S.R. Hyatt, R. Shunmugasundaram, J.R. Dahn, Studies of the capacity fade mechanisms of $LiCoO_2$/Si-alloy: Graphite cells, J. Electrochem. Soc. 163 (7) (2016) A1146.

[17] G.M. Veith, M. Doucet, R.L. Sacci, B. Vacaliuc, J.K. Baldwin, J.F. Browning, Determination of the solid electrolyte interphase structure grown on a silicon electrode using a fluoroethylene carbonate additive, Sci. Rep. 7 (1) (2017) 6326.

[18] Y. Jin, N.-J.H. Kneusels, P.C.M.M. Magusin, G. Kim, E. Castillo-Martínez, L.E. Marbella, R.N. Kerber, D.J. Howe, S. Paul, T. Liu, C.P. Grey, Identifying the structural basis for the increased stability of the solid electrolyte interphase formed on silicon with the additive fluoroethylene carbonate, J. Am. Chem. 139 (42) (2017) 14992–15004.

[19] G.G. Eshetu, E. Figgemeier, Confronting the challenges of next-generation silicon anode-based lithium-ion batteries: Role of designer electrolyte additives and polymeric binders, ChemSusChem 12 (12) (2019) 2515–2539.

[20] Y. Jin, N.-J.H. Kneusels, L.E. Marbella, E. Castillo-Martínez, P.C.M.M. Magusin, R.S. Weatherup, E. Jónsson, T. Liu, S. Paul, C.P. Grey, Understanding fluoroethylene carbonate and vinylene carbonate based electrolytes for Si anodes in lithium ion batteries with NMR spectroscopy, J. Am. Chem. Soc. 140 (31) (2018) 9854–9867.

[21] U.S. Vogl, S.F. Lux, E.J. Crumlin, Z. Liu, L. Terborg, M. Winter, R. Kostecki, The mechanism of SEI formation on a single crystal Si(100) electrode, J. Electrochem. Soc. 162 (4) (2015) A603.

[22] T. Hou, G. Yang, N.N. Rajput, J. Self, S.-W. Park, J. Nanda, K.A. Persson, The influence of fec on the solvation structure and reduction reaction of $LiPF_6$/EC electrolytes and its implication for solid electrolyte interphase formation, Nano Energy 64 (2019) 103881.

[23] A.M. Escamilla-Pérez, A. Roland, S. Giraud, C. Guiraud, H. Virieux, K. Demoulin, Y. Oudart, N. Louvain, L. Monconduit, Pitch-based carbon/nano-silicon composite, an efficient anode for Li-ion batteries, RSC Adv. 9 (19) (2019) 10546–10553.

[24] B.-C. Yu, Y. Hwa, J.-H. Kim, H.-J. Sohn, Carbon coating for Si nanomaterials as high-capacity lithium battery electrodes, Electrochem. Commun. 46 (2014) 144–147.

[25] M.C. Schulze, N.R. Neale, Half-cell cumulative efficiency forecasts full-cell capacity retention in lithium-ion batteries, ACS Energy Lett. 6 (3) (2021) 1082–1086.

[26] M.C. Schulze, G.M. Carroll, T.R. Martin, K. Sanchez-Rivera, F. Urias, N.R. Neale, Hydrophobic versus hydrophilic interfacial coatings on silicon nanoparticles teach us how to design the solid electrolyte interphase in silicon-based Li-ion battery anodes, ACS Appl. Energy Mater. 4 (2) (2021) 1628–1636.

[27] M.C. Schulze, K. Fink, J. Palmer, G.M. Carroll, N.S. Dutta, C. Zweifel, C. Engtrakul, S.-D. Han, N.R. Neale, B.J. Tremolet de Villers, Pitch carbon-coated ultrasmall Si nanoparticle lithium-ion battery anodes exhibiting reduced reactivity with carbonate-based electrolyte, Batter. Supercaps (2023a) page e202300186.

[28] K.U. Schwenke, S. Solchenbach, J. Demeaux, B.L. Lucht, H.A. Gasteiger, The impact of CO_2 evolved from VC and FEC during formation of graphite anodes in lithium-ion batteries, J. Electrochem. Soc. 166 (10) (2019) A2035.

[29] K. Kalaga, M.-T.F. Rodrigues, S.E. Trask, I.A. Shkrob, D.P. Abraham, Calendar-life versus cycle-life aging of lithium-ion cells with silicon-graphite composite electrodes, Electrochim. Acta 280 (2018) 221–228.

[30] C. Xu, F. Lindgren, B. Philippe, M. Gorgoi, F. Björefors, K. Edström, T. Gustafsson, Improved performance of the silicon anode for Li-ion batteries: Understanding the surface modification mechanism of fluoroethylene carbonate as an effective electrolyte additive, Chem. Mater. 27 (7) (2015) 2591–2599.

[31] C. Stetson, Y. Yin, C.-S. Jiang, S.C. DeCaluwe, M. Al-Jassim, N.R. Neale, C. Ban, A. Burrell, Temperature-dependent solubility of solid electrolyte interphase on silicon electrodes, ACS Energy Lett. 4 (12) (2019) 2770–2775.

[32] D.M. Seo, D. Chalasani, B.S. Parimalam, R. Kadam, M. Nie, B.L. Lucht, Reduction reactions of carbonate solvents for lithium ion batteries, ECS Electrochem. Lett. 3 (9) (2014) A91.

[33] E.J. Hopkins, S. Frisco, R.T. Pekarek, C. Stetson, Z. Huey, S. Harvey, X. Li, B. Key, C. Fang, G. Liu, G. Yang, G. Teeter, N.R. Neale, G.M. Veith, Examining CO_2 as an additive for solid electrolyte interphase formation on silicon anodes, J. Electrochem. Soc. 168 (3) (2021) 030534.

[34] A.L. Michan, B.S. Parimalam, M. Leskes, R.N. Kerber, T. Yoon, C.P. Grey, B.L. Lucht, Fluoroethylene carbonate and vinylene carbonate reduction: Understanding lithium-ion battery electrolyte additives and solid electrolyte interphase formation, Chem. Mater. 28 (22) (2016b) 8149–8159.

[35] J. Nanda, G. Yang, T. Hou, D.N. Voylov, X. Li, R.E. Ruther, M. Naguib, K. Persson, G.M. Veith, A.P. Sokolov, Unraveling the nanoscale heterogeneity of solid electrolyte interphase using tip-enhanced Raman spectroscopy, Joule 3 (8) (2019) 1–19.

[36] R. Petibon, L. Rotermund, K.J. Nelson, A.S. Gozdz, J. Xia, J.R. Dahn, Study of electrolyte components in Li ion cells using liquid-liquid extraction and gas chromatography coupled with mass spectrometry, J. Electrochem. Soc. 161 (6) (2014) A1167.

[37] Y. Jin, N.-J.H. Kneusels, C.P. Grey, NMR study of the degradation products of ethylene carbonate in silicon–lithium ion batteries, J. Phys. Chem. Lett. 10 (20) (2019) 6345–6350.

[38] F. Horsthemke, M. Leißing, V. Winkler, A. Friesen, L. Ibing, M. Winter, S. Nowak, Development of a lithium ion cell enabling in situ analyses of the electrolyte using gas chromatographic techniques, Electrochim. Acta 338 (2020) 135894.

[39] C.P. Aiken, J. Xia, D.Y. Wang, D.A. Stevens, S. Trussler, J.R. Dahn, An apparatus for the study of in situ gas evolution in Li-ion pouch cells, J. Electrochem. Soc. 161 (10) (2014) A1548.

[40] M. Leißing, C. Peschel, F. Horsthemke, S. Wiemers-Meyer, M. Winter, S. Nowak, The origin of gaseous decomposition products formed during SEI formation analyzed by isotope labeling in lithium-ion battery electrolytes, Batter. Supercaps 4 (11) (2021) 1731–1738.

[41] J.-P. Schmiegel, M. Leißing, F. Weddeling, F. Horsthemke, J. Reiter, Q. Fan, S. Nowak, M. Winter, T. Placke, Novel in situ gas formation analysis technique using a multilayer pouch bag lithium ion cell equipped with gas sampling port, J. Electrochem. Soc. 167 (6) (2020) 060516.

[42] P.J. Weddle, E.W.C. Spotte-Smith, A. Verma, H.D. Patel, K. Fink, B.J. Tremolet de Villers, M.C. Schulze, S.M. Blau, K. Smith, K. Persson, A. Colclasure, Continuum-level modeling of Li-ion battery SEI by upscaling atomistically informed reaction mechanisms, Electrochim. Acta 468 (2023) 143121.

[43] G.M. Carroll, M.C. Schulze, T.R. Martin, G.F. Pach, J.E. Coyle, G. Teeter, N.R. Neale, SiO_2 is wasted space in single-nanometer-scale silicon nanoparticle-based composite anodes for Li-ion electrochemical energy storage, ACS Appl. Energy Mater. 3 (11) (2020) 10993–11001.

[44] M.C. Schulze, M.-T.F. Rodrigues, J.D. McBrayer, D.P. Abraham, C.A. Apblett, I. Bloom, Z. Chen, A.M. Colclasure, A.R. Dunlop, C. Fang, K.L. Harrison, G. Liu, S.D. Minteer, N.R. Neale, D. Robertson, A.P. Tornheim, S.E. Trask, G.M. Veith, A. Verma, Z. Yang, C. Johnson, Critical evaluation of potentiostatic holds as accelerated predictors of capacity fade during calendar aging, J. Electrochem. Soc. 169 (5) (2022) 050531.

[45] A. Verma, M.C. Schulze, A. Colclasure, M.-T.F. Rodrigues, S.E. Trask, K. Pupek, C.S. Johnson, D.P. Abraham, Assessing electrolyte fluorination impact on calendar aging of blended silicon-graphite lithium-ion cells using potentiostatic holds, J. Electrochem. Soc. 170 (7) (2023) 070516.

[46] A. Verma, M.C. Schulze, A. Colclasure, M.-T.F. Rodrigues, S.E. Trask, K. Pupek, D.P. Abraham, Significant improvements to Si calendar lifetime using rapid electrolyte screening via potentiostatic holds, J. Electrochem. Soc. 171 (7) (2024) 070539.

[47] P.M. Attia, W.C. Chueh, S.J. Harris, Revisiting the $t^{0.5}$ dependence of SEI growth, J. Electrochem. Soc. 167 (9) (2020) 090535.

[48] I. Hasa, A.M. Haregewoin, L. Zhang, W.-Y. Tsai, J. Guo, G.M. Veith, P.N. Ross, R. Kostecki, Electrochemical reactivity and passivation of silicon thin-film electrodes in organic carbonate electrolytes, ACS Appl. Mater. Interf. 12 (36) (2020) 40879–40890.

[49] T. Liu, L. Lin, X. Bi, L. Tian, K. Yang, J. Liu, M. Li, Z. Chen, J. Lu, K. Amine, K. Xu, F. Pan, In situ quantification of interphasial chemistry in Li-ion battery, Nat. Nanotech. 14 (1) (2019) 50–56.

[50] R.T. Pekarek, A. Affolter, L.L. Baranowski, J. Coyle, T. Hou, E. Sivonxay, B.A. Smith, R.D. McAuliffe, K.A. Persson, B. Key, C. Apblett, G.M. Veith, N.R. Neale, Intrinsic chemical reactivity of solid-electrolyte interphase components in silicon–lithium alloy anode batteries probed by FTIR spectroscopy, J. Mater. Chem. A 8 (16) (2020) 7897–7906.

[51] G.V. Zhuang, H. Yang, P.N. Ross, K. Xu, T.R. Jow, Lithium methyl carbonate as a reaction product of metallic lithium and dimethyl carbonate, Electrochem. Solid-State Lett. 9 (2) (2005) A64.

[52] P. Ross, Studies of interfacial chemistry in lithium and Li-ion battery systems using infrared spectroscopy, ECS Trans. 1 (26) (2006) 161.

[53] S.K. Heiskanen, J. Kim, B.L. Lucht, Generation and evolution of the solid electrolyte interphase of lithium-ion batteries, Joule 3 (10) (2019) 2322–2333.

[54] V. Etacheri, O. Haik, Y. Goffer, G.A. Roberts, I.C. Stefan, R. Fasching, D. Aurbach, Effect of fluoroethylene carbonate (FEC) on the performance and surface chemistry of Si-nanowire Li-ion battery anodes, Langmuir 28 (1) (2012) 965–976.

[55] I.A. Shkrob, J.F. Wishart, D.P. Abraham, What makes fluoroethylene carbonate different? J. Phys. Chem. C 119 (27) (2015) 14954–14964.

[56] B. Strehle, S. Solchenbach, M. Metzger, K.U. Schwenke, H.A. Gasteiger, The effect of CO_2 on alkyl carbonate trans-esterification during formation of graphite electrodes in Li-ion batteries, J. Electrochem. Soc. 164 (12) (2017) A2513.

[57] C. Peschel, F. Horsthemke, M. Leißing, S. Wiemers-Meyer, J. Henschel, M. Winter, S. Nowak, Analysis of carbonate decomposition during solid electrolyte interphase formation in isotope-labeled lithium ion battery electrolytes: Extending the knowledge about electrolyte soluble species, Batter. Supercaps 3 (11) (2020) 1183–1192.

[58] S.S. Zhang, A review on electrolyte additives for lithium-ion batteries, J. Power Sources 162 (2) (2006) 1379–1394.

[59] L. Bläubaum, P. Röse, L. Schmidt, U. Krewer, The effects of gas saturation of electrolytes on the performance and durability of lithium-ion batteries, ChemSusChem 14 (14) (2021) 2943–2951.
[60] D.M. Seo, O. Borodin, D. Balogh, M. O'Connell, Q. Ly, S.-D. Han, S. Passerini, W.A. Henderson, Electrolyte solvation and ionic association III. Acetonitrile-lithium salt mixtures–transport properties, J. Electrochem. Soc. 160 (8) (2013) A1061–A1070.
[61] L.D. Ellis, J.P. Allen, L.M. Thompson, J.E. Harlow, W.J. Stone, I.G. Hill, J.R. Dahn, Quantifying, understanding and evaluating the effects of gas consumption in lithium-ion cells, J. Electrochem. Soc. 164 (14) (2017) A3518.
[62] M. Soto, K. Fink, C. Zweifel, P.J. Weddle, E.W.C. Spotte-Smith, G.M. Veith, K.A. Persson, A.M. Colclasure, B.J. Tremolet de Villers, Solubilities of ethylene and carbon dioxide gases in lithium-ion battery electrolyte, J. Chem. Engin. Data 69 (6) (2024) 2236–2243.
[63] K.L. Browning, L. Baggetto, R.R. Unocic, N.J. Dudney, G.M. Veith, Gas evolution from cathode materials: A pathway to solvent decomposition concomitant to SEI formation, J. Power Sources 239 (2013) 341–346.
[64] Y. Ha, C. Stetson, S.P. Harvey, G. Teeter, B.J. Tremolet de Villers, C.-S. Jiang, M. Schnabel, P. Stradins, A. Burrell, S.-D. Han, Effect of water concentration in $LiPF_6$-based electrolytes on the formation, evolution, and properties of the solid electrolyte interphase on Si anodes, ACS Appl. Mater. Interf. 12 (44) (2020) 49563–49573.
[65] G. Zhuang, Y. Chen, P.N. Ross, The reaction of lithium with carbon dioxide studied by photoelectron spectroscopy, Surf. Sci. 418 (1) (1998) 139–149.
[66] L. Chen, K. Wang, X. Xie, J. Xie, Enhancing electrochemical performance of silicon film anode by vinylene carbonate electrolyte additive, Electrochem. Solid-State Lett. 9 (11) (2006) A512.
[67] B. Kumru, N. Bicak, Synthesis of soluble poly(vinylene carbonate) by redox-initiated RAFT process in microemulsion and its aminolysis yielding snow-white polymethylol, RSC Adv. 5 (39) (2015) 30936–30942.
[68] B. Apicella, A. Tregrossi, F. Stazione, A. Ciajolo, C. Russo, Analysis of petroleum and coal tar pitches as large PAH, Chem. Eng. Trans. 57 (2017) 775–780.
[69] K.A. See, M.A. Lumley, G.D. Stucky, C.P. Grey, R. Seshadri, Reversible capacity of conductive carbon additives at low potentials: Caveats for testing alternative anode materials for Li-ion batteries, J. Electrochem. Soc. 164 (2) (2016) A327.
[70] Z. Huey, M.C. Schulze, G.M. Carroll, C. Engtrakul, C.-S. Jiang, S.C. DeCaluwe, B.J. Tremolet de Villers, S.-D. Han, Characterization of pitch carbon coating properties affecting the electrochemical behavior of silicon nanoparticle lithium-ion battery anodes, J. Mater. Chem. A 12 (44) (2024) 30465–30475.
[71] Y. An, Y. Tian, C. Liu, S. Xiong, J. Feng, Y. Qian, One-step, vacuum-assisted construction of micrometer-sized nanoporous silicon confined by uniform two-dimensional N-doped carbon toward advanced Li ion and MXene-based Li metal batteries, ACS Nano 16 (3) (2022) 4560–4577.
[72] Y. Tian, Z. Pei, D. Luan, X.W.D. Lou, Anchoring Sn nanoparticles in Necklace-Like B, N, F-doped carbon fibers enables anode-less 5V-class Li-metal batteries, Angew. Chem. Int. Ed. 64 (13) e202423454.